Flux Noise due to Spins in SQUIDs

by

Stephanie LaForest
B.Sc., Queen's University, 2011

A Thesis Submitted in Partial Fulfillment of the
Requirements for the Degree of

MASTERS OF SCIENCE

in the Department of Physics and Astronomy

Flux Noise due to Spins in SQUIDs

by

Stephanie LaForest
B.Sc., Queen's University, 2011

Supervisory Committee

Dr. Rogério de Sousa, Supervisor
(Department of Physics and Astronomy)

Dr. Pavel Kovtun, Departmental Member
(Department of Physics and Astronomy)

Supervisory Committee

Dr. Rogério de Sousa, Supervisor
(Department of Physics and Astronomy)

Dr. Pavel Kovtun, Departmental Member
(Department of Physics and Astronomy)

ABSTRACT

Superconducting Quantum Interference Devices (SQUIDs) are currently being used as flux qubits and read-out detectors in a variety of solid-state quantum computer architectures. The main limitation of SQUID qubits is that they have a coherence time of the order of 10 μs, due to the presence of intrinsic flux noise that is not yet fully understood. The origin of flux noise is currently believed to be related to spin impurities present in the materials and interfaces that form the device. Here we present a novel numerical method that enables calculations of the flux produced by spin impurities even when they are located quite close to the SQUID wire. We show that the SQUID will be particularly sensitive to spins located at its wire edges, generating flux shifts of up to 4 nano flux quanta, much higher than previous calculations based on the software package FastHenry. This shows that spin impurities in a particular region along the wire's surface play a much more important role in producing flux noise than other spin impurities located elsewhere in the device.

Contents

List of Figures

ACKNOWLEDGEMENTS

I would like to thank:

My family and friends for their love and support.

Drs. Mohammad Amin and Trevor Lanting of D-Wave Systems, Inc. for the opportunity to work with them.

The other Physics graduate students at the University of Victoria for their inspiration, guidance, and friendship.

Dr. Rogério de Sousa for his patience and insight into my thesis project, and for keeping me focused when at times I was in need of motivation.

DEDICATION

To my Father, Stephen LaForest

Chapter 1

Introduction

SQUIDs (Superconducting Quantum Interference Devices) are highly sensitive magnetometers. Their ability to detect fields as low as 10^{-15} T makes them ideal for use in many applications in different scientific areas. However, this high degree of sensitivity also causes the SQUIDs to be very sensitive to intrinsic noise. Magnetic field fluctuations caused by spins in the surrounding material is one possible source of noise and is currently believed to be the dominant one [24, 9, 3]. In this thesis, I present two methods of calculating the flux caused by a single spin in a SQUID. The first is a software package called FastHenry which computes the self-and mutual inductances of a superconducting geometry based on London's equations. The second is an exact integration method which treats the spin as a dipole but neglects the Meissner effect.

The principles of superconductivity are essential in understanding how a SQUID works. Here is presented an introduction to the Physics behind superconductivity followed by a brief overview of quantum computing and the use of a SQUID in this field.

1.1 Superconductivity

Superconductivity, discovered by H. Kamerling Onnes in 1911 [21], is a phenomenon which occurs in several materials at very low temperatures. In normal metals, as the temperature is lowered, the resistance of the metal decreases gradually. In superconducting materials, as the temperature is lowered, the resistance of the metal decreases gradually until reaching a specific temperature called the ciritical temperature. At

this critical temperature, T_C, the resistivity drops to zero as shown in Figure 1.1. The first notable characteristic of superconductors is that below T_C, they exhibit perfect conductivity [29].

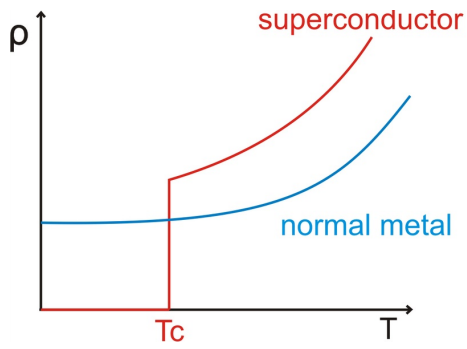

Figure 1.1: Temperature dependence of the resistance of a superconductor and a normal metal.

The second electrodynamic property that is characteristic of superconductivity is the Meissner effect, which was found in 1933 by Meissner and Ochsenfeld [20]. When a superconductor is in the presence of an external constant applied magnetic field, the magnetic field is ejected from the superconductor as it is cooled through the transition temperature. An illustration of this effect is shown in Figure 1.2. The superconductor expels the external magnetic field by creating a screening current to counteract that caused by the magnetic field. In doing this, all of the flux through the interior of the superconductor is cancelled, and the superconductor becomes perfectly diamagnetic.

It should be remarked that the Meissner effect is a unique property of the superconducting state, and is a property that is independent of its zero resistance. In fact, a non-superconducting metal can, in principle, have zero resistance at low temperatures. However, the magnetic field will always penetrate into the non-superconducting metal.

These two properties which are unique to superconductivity were described in 1935 by brothers F. and H. London [17], who proposed two equations to describe electric and magnetic fields applied to a superconductor. The two London equations for the electric field $\vec{E}$ and magnetic field $\vec{B}$ within the superconductor are

$$\vec{E} = \frac{\partial}{\partial t}(\Lambda \vec{j}_s) \tag{1.1}$$

and

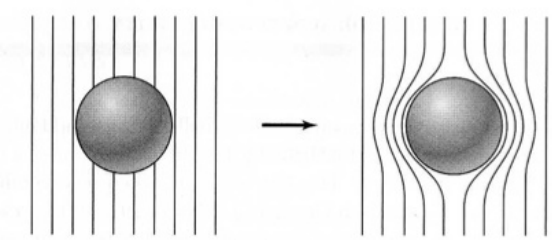

Figure 1.2: The Meissner effect in a sphere of superconducting material. As the superconductor passes through the transition temperature, the external magnetic field is expelled[16].

$$\vec{B} = -\nabla \times (\Lambda \vec{j_s}) \tag{1.2}$$

where Λ is a parameter given by

$$\Lambda = \frac{m}{n_s e^2}. \tag{1.3}$$

Here, m is the electron mass, n_s is the number density of superconducting electrons, and $\vec{j_s}$ is the superconducting current density. Perfect conductivity is described by the first London equation, since the electric field accelerates superconducting electrons against resistance, in contrast to Ohm's law where the velocity of the electrons is kept constant. The second London equation describes the Meissner effect. This can be seen by plugging Ampere's Law,

$$\nabla \times \vec{B} = \mu_0 \vec{j} \tag{1.4}$$

into Eq. 1.2. This results in the differential equation

$$\nabla^2 \vec{B} = \frac{1}{\lambda^2} \vec{B} \tag{1.5}$$

where

$$\lambda^2 = \frac{\Lambda}{\mu_0} = \frac{m}{\mu_0 n_s e^2} \tag{1.6}$$

is a parameter specific to the superconductor called the penetration depth. This implies that a magnetic field is screened exponentially from inside the syperconductor, and can only penetrate within a distance of the penetration depth, λ, thus describing the Meissner effect.

In 1957, the BCS (Bardeen-Cooper-Schreiffer) developed a microscopic theory to explain superconductivity [12]. BCS theory shows that two electrons in a lattice can couple through lattice vibrations in order to form what is called a Cooper pair. Normally, electrons repel eachother due to their negative charge. However, according to BCS theory, as a negatively charged electron moves through a lattice, the positive charges in the lattice cause the lattice to distort, forming a shield of positive charges around the electron. This effectively gives the electron a positive charge, allowing it to pair with another electron of negative charge, separated by hundreds of nanometers. An illustration of a Cooper pair moving through a lattice is shown in Figure 1.3.

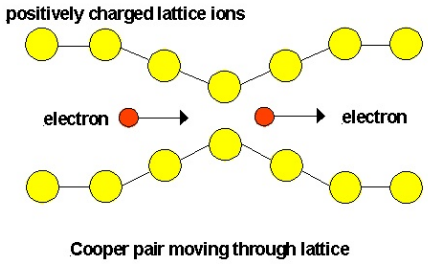

Figure 1.3: Illustration of the lattice distortion due to a negatively charged electron, which allows electrons to couple into Cooper pairs.

Cooper pairs stay together because of an exchange where one electron interacts with a positive lattice atom, causing a lattice vibration or emitting a phonon. Then the phonon travels through the lattice and is absorbed by the other atom in the pair. In reality, Cooper pairs are constantly breaking and recombining, but because electrons are indistinguishable they can be considered to be coupled permanently. It is these pairs which allow electrons to move through the lattice where there would normally be resistance.

If the electrons gain sufficient energy, the Cooper pairs will break apart, putting the superconductor into a resistive state. This can occur above T_C, or below T_C if there is sufficient current through the superconductor. Thus, there is a maximum value for the magnetic field, known as the critical magnetic field H_C, which is temperature dependent. For all superconducting materials, there are specific conditions of temperature and applied magnetic field that are needed in order for the material to be in its superconducting state. For all other conditions, the material behaves as a normal conductor. Typical superconductors have T_C between 1 and 23 K, while there are high temperature superconductors with T_C between 90 and 138 K which

were discovered more recently.

An important property of Cooper pairs is that pairs can tunnel between two superconductors separated by what is called a weak link. The weak link could be an insulating layer, or a layer with low conductivity which separates two superconducting segments. A junction of this type is called a Josephson junction and is shown in Figure 1.4.

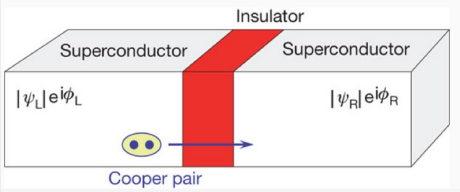

Figure 1.4: A Josephson Junction. Cooper pairs tunnel through a thin insulating layer between two superconductors.

1.1.1 Theoretical Derivation of the Josephson Relations

Josephson was the first to predict the tunneling of Cooper pairs, which occurs even if there is no voltage difference across the barrier. The Ginzburg-Landau (G-L) theory can be used to derive the Josephson relations, which give rise to this effect. The G-L theory is an approximate theory, where the superconductor can be described by a single wave function,

$$\psi(\vec{r},t) = |\psi|e^{i\phi} \tag{1.7}$$

where $|\psi_s|^2 = n_s$ is the Cooper pair density, and $\psi(\vec{r},t)$ is the phase. This wave function gives a mean-field representation of the Cooper pair centre of mass wave function.

Consider a Josephson junction in a superconducting wire, connected to two voltage sources as in Figure 1.5. For distances where the length of the junction, L, is much less than ξ, the coherence length in G-L theory, the Ginzburg Landau equation can be approximated by

$$-\frac{\hbar^2}{2m*}\nabla^2\psi \approx 0\,. \tag{1.8}$$

The coherence length is a parameter which describes the variation of the density in the superconducting material. In this approximation, ψ behaves similar to a single quantum particle in free space with energy equal to zero, in the absence of electric and

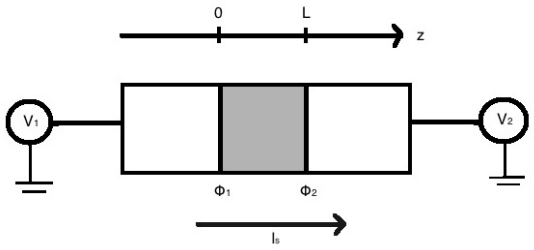

Figure 1.5: A Josephson junction of length L in a superconducting material with two voltages applied to each end. The phase difference across the junction is $\phi_2 - \phi_1$.

magnetic fields[29]. The solution to Eq. 1.8 is the solution to the Laplace equation, given by

$$\psi(z) = a + bz\,. \tag{1.9}$$

The constants a and b can be determined by noting that when the superconductors on either side of the junction are in equilibrium, we can impose

$$|\psi(z=0)| = |\psi(z=L)| = |\psi_\infty|\,, \tag{1.10}$$

with $|\psi_\infty| = \sqrt{n_s}$, in the middle of each superconductor. Because the wave functions across the junction may differ only in phase, we have the boundary conditions

$$\begin{aligned} \psi(z=0) &= |\psi_\infty| e^{i\phi_1}\,, \\ \psi(z=L) &= |\psi_\infty| e^{i\phi_2} \end{aligned} \tag{1.11}$$

which give the unique solution

$$\psi(z) = |\psi_\infty| \left[\left(1 - \frac{z}{L}\right) e^{i\phi_1} + \left(\frac{z}{L}\right) e^{i\phi_2} \right]. \tag{1.12}$$

The supercurrent can then be determined by the quantum mechanical current relation

$$\frac{\partial [q^* |\psi|^2]}{\partial t} = -\vec{\nabla} \cdot \vec{J}, \tag{1.13}$$

where q^* is the charge of the Cooper pairs. Using this, we have

$$\begin{aligned}\vec{J} &= \frac{q^*\hbar}{2m^*i}[\psi^*\vec{\nabla}\psi - \psi\vec{\nabla}\psi^*] \\ &= \frac{q^*\hbar}{m}\mathrm{Im}(\psi^*\vec{\nabla}\psi)\,.\end{aligned} \tag{1.14}$$

This is valid for $\vec{E} = \vec{B} = 0$, $\vec{A} = 0$, and gives

$$\begin{aligned}J_z &= \frac{q^*\hbar}{m^*}|\psi_\infty|^2\mathrm{Im}\left\{\left[\left(1-\frac{z}{L}\right)e^{-i\phi_1} + \left(\frac{z}{L}\right)e^{-i\phi_2}\right]\left[\frac{-1}{L}e^{i\phi_1} + \frac{1}{L}e^{i\phi_2}\right]\right\} \\ &= \frac{q^*\hbar}{m^*}|\psi_\infty|^2\mathrm{Im}\left\{\frac{-1}{L}\left(1-\frac{z}{L}\right) + \frac{1}{L}\left(1-\frac{z}{L}\right)e^{-i(\phi_1-\phi_2)} - \left(\frac{z}{L^2}\right)e^{i(\phi_1-\phi_2)} + \left(\frac{z}{L^2}\right)\right\} \\ &= \frac{q^*\hbar}{m^*}|\psi_\infty|^2\left\{\frac{1}{L}\left(1-\frac{z}{L}\right)\sin(\phi_2-\phi_1) + \left(\frac{z}{L^2}\right)\sin(\phi_2-\phi_1)\right\}\end{aligned} \tag{1.15}$$

which reduces to

$$J_z = \frac{q^*\hbar}{m^*L}|\psi_\infty|^2\sin(\phi_2-\phi_1)\,. \tag{1.16}$$

From this, the supercurrent is determined to be

$$I_s = I_c\sin(\phi_2-\phi_1)\,, \tag{1.17}$$

called the first Josephson relation. Here,

$$I_c = \frac{Aq^*\hbar}{m^*L} \approx \frac{2e\hbar}{2m_e^*L} \tag{1.18}$$

is the critical current of the junction where A is the area of the junction, and $m^* = 2m_e^*$ is the Cooper pair mass, twice the single electron effective mass of the metal. The Josephson junction usually has a critical current that is less than that of the two surrounding superconductors. This is called the DC Josephson effect.

The AC Josephson effect occurs when a direct voltage, V, is applied across the junction, causing the phase difference to increase with time. This generates an oscillating current flow with frequency $\omega = 2eV/\hbar$. Again, there is a maximum voltage, V_C, that can be applied which would cause the cooper pairs to break apart across the link and the junction to move into the resistive state. This effect is described by the

second Josephson relation.

The second Josephson relation can be derived by analyzing the dynamics of ψ. We can write

$$\psi(\vec{r},t) = \psi(\vec{r},0)e^{\frac{-iE_{Cooper}t}{\hbar}}\,, \tag{1.19}$$

as ψ is taken to be the wave function of the centre of mass of a Cooper pair. The energy of Cooper pairs is close to the Fermi level, so $E_{Cooper} = 2\epsilon_F$. When a superconductor is in equilibrium, $|\psi| = \sqrt{n_s}$ does not depend on time, thus the time dependence is due to the phase:

$$\phi(\vec{r},t) = \phi(\vec{r},0) = \frac{2\epsilon_F t}{\hbar}\,, \tag{1.20}$$

which can be written as

$$\frac{\partial\phi}{\partial t} = -\frac{2\epsilon_F}{\hbar} = -\frac{2}{\hbar}[\epsilon_F(V=0) + eV(\vec{r})]\,, \tag{1.21}$$

where $V(\vec{r})$ is the voltage at point $\vec{r}$, and $e < 0$ is the electron charge. Now applying this to our junction,

$$\frac{\partial\phi_1}{\partial t} = -\frac{2}{\hbar}[\epsilon_F(V=0) + eV_1] \tag{1.22}$$

and

$$\frac{\partial\phi_2}{\partial t} = -\frac{2}{\hbar}[\epsilon_F(V=0) + eV_2]\,. \tag{1.23}$$

Combining Eqs.1.22 and 1.23 into one equation results in the second Josephson relation;

$$\frac{\partial\phi}{\partial t} = -\frac{2e}{\hbar}V\,, \tag{1.24}$$

where $\phi = (\phi_2 - \phi_1)$ and $V = (V_2 - V_1)$[14].

Josephson junctions are essential elements in superconducting devices. Both the AC and DC Josephson effects are important in understanding the function of a SQUID, which is presented in the next chapter. First, I will go into more detail about the Cooper pair energy in a Josephson junction by looking at the wave function.

1.1.2 Quantization of the Josephson Junction

In this section I will show that the energy levels in a Josephson junction are quantized by deriving an orthonormal basis for the junction wave functions. To start, let's calculate the energy stored in a Josephson junction as in figure 1.5 with $V_2 - V_1$ when the phase is changed from $\phi = 0$ to ϕ. This establishes a supercurrent I_s. The work required to move elements of charge dq across the junction from voltage source 1 to 2 is:

$$W = \int_{\phi=0}^{\phi} (\delta q)(V_2 - V_1) = \int \frac{\delta q}{dt}(V_2 - V_1)dt\,. \tag{1.25}$$

Implementing the Josephson relations,

$$\frac{\delta q}{dt} = I_s = I_c \sin(\phi) \tag{1.26}$$

and

$$\frac{\hbar}{2e}\frac{d\phi}{dt} = V_2 - V_1\,, \tag{1.27}$$

we have

$$W = \left(\frac{\hbar I_c}{2e}\right)\int_0^{\phi} \sin(\phi)d\phi = E_J[-\cos(\phi) + 1]\,, \tag{1.28}$$

where $E_J = \frac{\hbar I_c}{2e}$ is the Josephson energy. Hence, the potential energy stored in the Josephson junction with phase difference ϕ can be written as

$$U = -E_J \cos(\phi)\,. \tag{1.29}$$

The kinetic energy analogue of the junction is the sum of the electrostatic energy in the superconductors. The kinetic energy for each individual superconductor is

$$T_i = \frac{(2en_i)^2}{2C_i} = \frac{1}{2}C_i V_i^2 = \frac{1}{2}C_i\left(\frac{-\hbar}{2e}\dot{\phi}_i\right)^2 = \frac{1}{2}\frac{C_i}{(2e)^2}(\hbar\dot{\phi}_i)^2\,, \tag{1.30}$$

where n_i is the number of Cooper pairs in excess of charge neutrality, and C_i is the capacitance of each superconductor ($i = 1, 2$). We can define effective coordinates and masses for our problem,

$$x_i = \hbar\phi_i \,,\; m_i = \frac{C_i}{(2e)^2} \tag{1.31}$$

such that

$$T_i = \frac{1}{2} m_i (\dot{x}_i)^2 \,. \tag{1.32}$$

Here, m_i has dimension of Energy^{-1} and $\dot{x}_i$ has dimension of energy. Using these coordinates, we can write the Lagrangian for the system:

$$L(x_1, x_2, \dot{x}_1, \dot{x}_2) = \sum_{i=1,2} \frac{1}{2} m_i \dot{x}_i^2 + E_J \cos\left(\frac{x_2 - x_1}{\hbar}\right) \,. \tag{1.33}$$

The associated canonical momentum is

$$p_i = \frac{\partial L}{\partial \dot{x}_i} = m_i \dot{x}_i = \frac{C_i}{(2e)^2} \hbar \dot{\phi}_i = \frac{\hbar C_i}{(2e)^2} \frac{(-2e)}{\hbar} V_i \,. \tag{1.34}$$

Because $V_i = \frac{2en_i}{C_i}$, the momentum simplifies to

$$p_i = -n_i \,. \tag{1.35}$$

We can now apply the correspondence principle, which states that in the limit of large numbers quantum theory reproduces classical mechanics, to quantize the problem. Define the operators $\hat{x}_i$ and $\hat{p}_i$ such that

$$[\hat{x}_i, \hat{p}_j] = i\hbar\delta_{ij} \,, \tag{1.36}$$

or

$$[\hat{\phi}_i, \hat{n}_j] = i\delta_{ij} \tag{1.37}$$

so that the phase and Cooper pair number are conjugate quantum operators, just like the position and momentum of a particle in one dimension. In the phase representation, the state of the Josephson junction is represented by a wave function $\psi(\phi_i)$ that depends only on the phase, with

$$\hat{n}_i = -\hat{p}_i = -\frac{\hbar}{i}\frac{\partial}{\partial x_i} = i\frac{\partial}{\partial \phi_i} \,. \tag{1.38}$$

We can check this by applying the phase-Cooper pair number relation to ψ:

$$[\hat{\phi}_i, \hat{n}_i]\psi = [\phi_i, i\frac{\partial}{\partial\phi_i}]\psi(\phi_i) = \phi_i i\frac{\partial}{\partial\phi_i}\psi - i\frac{\partial}{\partial\phi_i}(\phi_i\psi) = -i\psi\,. \tag{1.39}$$

This state obeys the following normalization condition:

$$\int_{-\pi}^{\pi} d\phi_i |\psi(\phi_i)|^2 = 1\,. \tag{1.40}$$

The eigenstates of $\hat{n}_i$ form a possible orthonormal basis for the Josephson junction:

$$\psi_{n_i}(\phi_i) = \langle\phi_i|n_i\rangle = \frac{1}{\sqrt{2\pi}} e^{-in_i\phi_i}\,,\ (n_i = -\infty, ..., -1, 0, 1, 2, ..., \infty)\,. \tag{1.41}$$

Note that n_i must be integers so that $\psi_{n_i}(\phi_i + 2\pi m) = \psi_{n_i}(\phi_i)$ for any integer m. From this we can see that the energy of a Josephson junction must be quantized.

1.2 SQUIDs

1.2.1 What is a SQUID

A SQUID (Superconducting Quantum Interference Device) is an extremely sensitive magnetometer used in fields such as Physics, Biology, and Neuroscience. SQUIDs can measure magnetic fields as low as 5×10^{-15} T, which is smaller than the magnetic field caused by the brain's neuron current signals. A DC SQUID consists of a closed loop of superconducting material with two thin insulating layers which form two Josephson junctions in parallel, as shown in Figure 1.6.

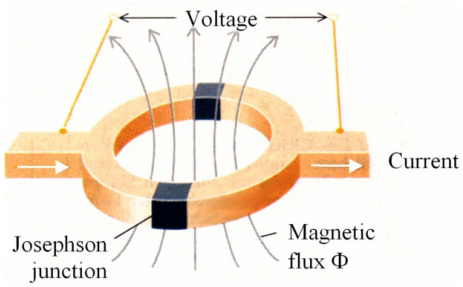

Figure 1.6: A DC SQUID. Two Josephson junctions connected in parallel on a closed superconducting loop.

SQUIDs work by exploiting the property that superconducting rings can enclose

magnetic flux only in multiples of the flux quantum, a universal constant Φ_0 which is defined by $\Phi_0 = h/2e$ where e is the charge of an electron and h is Planck's constant. The flux quantum is the smallest quantity of flux, which explains how SQUIDs can be so sensitive. This sensitivity is also what causes measurements from SQUIDs to be strongly affected by background noise. Figure 1.7 shows the frequency dependent noise spectrum for an experimental measure of noise in SQUIDs.

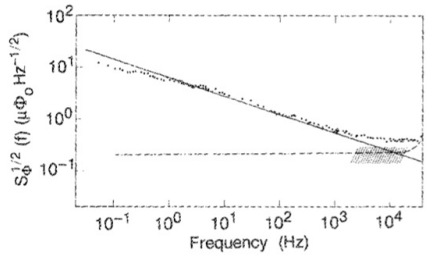

Figure 1.7: The rms flux noise in a DC-SQUID measured at 90mK [30]

Determining the quantity and sources of flux noise can lead to reductions in the amount of noise and improvements in readings. SQUIDs are essentially flux-to-voltage transducers which convert detected magnetic flux through the center of the loop into voltage which can be more easily measured.

1.2.2 How a DC SQUID Works

Essential to the function of a SQUID is the principle that the total magnetic flux that passes through a superconducting ring is quantized. This is a truly quantum effect that leads to observable consequences on a macroscopic (many electron) level.

Electrons are spin-1/2 fermions, but in a superconductor they pair up forming a Cooper pair of spin-0. Hence the electrons behave as a free boson gas of charged particles. Taking $\psi(r)$ to be the wave function of the boson and $n = \psi * \psi = |\psi|^2$ to be the concentration of cooper pairs, then the wave function can be written as

$$\psi(r) = \sqrt{n}e^{i\phi} \tag{1.42}$$

where ϕ is the phase. From the Hamilton equation for the momentum, $\mathbf{p}$, of a charged particle in an electromagnetic field, the velocity operator of a particle is

$$\mathbf{v} = \frac{1}{m}\left(\mathbf{p} - q\vec{A}\right) = \frac{1}{m}\left(-i\hbar\nabla - q\vec{A}\right) \tag{1.43}$$

where $\vec{A}$ is the magnetic vector potential, and q is the charge of the particle, which in this case is $2e$ for the Cooper pair ($e < 0$). Classically, current density is defined according to the equation

$$\vec{j} = nq\vec{v}. \tag{1.44}$$

Replacing $n\vec{v}$ by the expectation value of the $\mathbf{v}$ operator in order to treat the problem quantum mechanically gives

$$\vec{j} = q\psi^* \mathbf{v} \psi = \frac{nq}{m}\left(\hbar\nabla\phi - q\vec{A}\right), \tag{1.45}$$

where we assumed that n is uniform (independent of r), but ϕ is space dependent. It can be seen by taking the curl of both sides that this agrees with the London equation $\vec{B} = -\nabla \times (\Lambda j_s)$.

We can choose a closed path C through the center of the superconducting material forming a loop as shown in Figure 1.8.

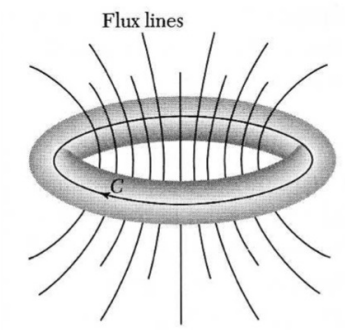

Figure 1.8: The path of integration through the center of the material in a superconducting ring. The flux through the ring is quantized in units of Φ_0 [16].

According the the Meissner effect, both $\vec{B}$ and j are zero in the interior of the material. It can be seen from Eq. 1.45 that this occurs when the following condition is met:

$$\hbar\nabla\phi = q\vec{A}. \tag{1.46}$$

Taking the integral of the phase change of the pairs around the closed loop gives

$$q\oint_C \vec{A}\cdot dl = \hbar\oint_C \nabla\phi \cdot dl = \hbar(\phi_2 - \phi_1). \tag{1.47}$$

Since ψ must be single-valued, we have

$$\phi_2 - \phi_1 = 2\pi m \tag{1.48}$$

where m is an integer. Now applying Stokes' theorem to the left side of Eq. 1.47 gives

$$\oint_C \vec{A} \cdot dl = \int_C (\nabla \times \vec{A}) \cdot da = \int_C \vec{B} \cdot da \tag{1.49}$$

where da is the area element, and

$$\Phi = \int_C \vec{B} \cdot da \tag{1.50}$$

is the definition of the magnetic flux through C. Based on the condition of Eq. 1.48 and using $q = 2e$, we get

$$\Phi = m\frac{h}{2e} = m\Phi_0\,, \tag{1.51}$$

where $\Phi_0 = h/2e$ is the flux quantum. Therefore, the flux through the superconducting ring is quantized in integer multiples of Φ_0 [29].

This is an example of the Aharonov-Bohm effect [26]. This effect is a quantum-mechanical phenomenon where a charged particle is affected by a magnetic field even when in an area where both the magnetic and electric fields are zero. This can occur because although the magnetic field is zero in the region, the vector potential is non-zero, which in this case, induces a phase shift in the wave function of the charged particles.

The total flux through the superconducting ring is a combination of the flux from external magnetic fields and the flux from the superconducting currents which flow in the ring. The phase difference is given in terms of the total flux by

$$\phi_2 - \phi_1 = 2\pi\frac{\Phi}{\Phi_0}(\mathrm{mod}2\pi)\,. \tag{1.52}$$

Now consider a DC-SQUID with two Josephson junctions in parallel, with currents I_a and I_b passing through each junction as shown in Figure 1.9. The phase difference taken on a path through junction a is labelled δ_a, and the phase difference taken on a path through junction b is δ_b. Integrating Eq. 1.46 over the two disconnected paths inside the superconductor yields

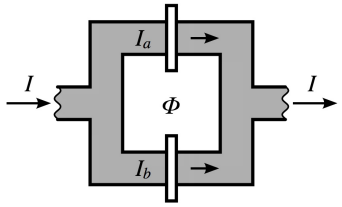

Figure 1.9: A magnetic flux Φ passes through the interior of a superconducting loop with two Josephson Junctions, with total current I through the circuit.

$$\delta_b - \delta_a = 2\pi \frac{\Phi}{\Phi_0} (\text{mod} 2\pi). \tag{1.53}$$

Manipulating this to give

$$\delta_b = \delta_0 + \pi \frac{\Phi}{\Phi_0}, \text{ and } \delta_a = \delta_0 - \pi \frac{\Phi}{\Phi_0}, \tag{1.54}$$

where δ_0 is the phase change across each junction when $\Phi = 0$, assuming that the two junctions are identical. The total current of the SQUID is the sum of the currents passing through each junction. Based on Eq. 1.17 for the current through a Josephson junction, the total current through the SQUID is

$$\begin{aligned} I_{total} &= I_c \left\{ \sin\left(\delta_0 + \pi \frac{\Phi}{\Phi_0}\right) + \sin\left(\delta_0 - \pi \frac{\Phi}{\Phi_0}\right) \right\} \\ &= 2(I_c \sin\delta_0) \cos\left(\pi \frac{\Phi}{\Phi_0}\right) \end{aligned} \tag{1.55}$$

So the expression for the maximum supercurrent flowing through the SQUID is given by

$$I_m = 2I_c \left| \cos\left(\pi \frac{\Phi}{\Phi_0}\right) \right| \tag{1.56}$$

which has maxima when Φ/Φ_0 is an integer. This relation is shown in Figure 1.10.

To understand how a DC-SQUID works, consider a squid biased with a current I through a device with two identical junctions. The bias current splits across the two junctions so that the critical current of the SQUID is now twice the critical current of one of its junctions. When an external magnetic field is applied to a SQUID, a screening current, I_s is generated to oppose this magnetic field according to the Meissner effect. This will increase the total current through one junction, and

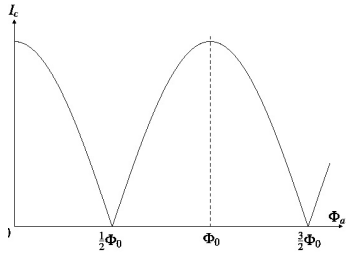

Figure 1.10: The maximum supercurrent as a function of the flux through the center of the SQUID loop.

decrease the total current through the other as shown in Figure 1.11. The applied magnetic field lowers the critical current of the SQUID by $2I_s$, as the total current through one of the junctions has now been raised. This means that less current can be passed through the junction before it becomes resistive, causing the whole loop to be resistive. The total flux through the ring is a combination of the flux from external sources, and the flux due to the current through the ring. The screening current will adjust itself in order to keep the total flux quantized.

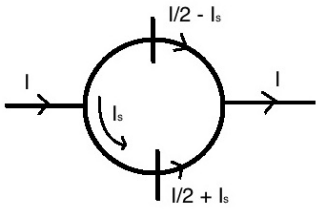

Figure 1.11: Schematic drawing of the currents through each junction in a DC-SQUID when a bias current I is applied. The screening current, I_s, is generated to oppose the flux of an external magnetic field, which decreases the critical current of the SQUID.

SQUID magnetometers are biased with current that is slightly greater than the critical current, so that the device always operates in a resistive mode and a voltage can be registered across the SQUID. When the flux inside the loop reaches one flux quantum, the screening current vanishes, restoring the superconductivity of the loop momentarily, allowing one quantum of magnetic flux to enter. If the magnetic flux continues to increase to another half flux quantum, instead of increasing, it is now energetically preferable for the screening current to increase the enclosed flux to a multiple of one flux quantum. The screening current will decrease and change direction. Thus, the screening current changes direction every half flux quantum. It is periodic in ϕ with period ϕ_0 (Figure 1.12), as is the voltage that can now be measured

across the device. This voltage is determined as a function of the bias current and the maximum supercurrent by

$$\begin{aligned} V &= \frac{R}{2}\sqrt{I^2 - I_m^2} \\ &= \frac{R}{2}\left\{ I^2 - \left[2I_c \cos\left(\pi \frac{\Phi}{\Phi_0} \right) \right]^2 \right\}^{1/2} . \end{aligned} \tag{1.57}$$

This voltage-flux relation is displayed in Figure 1.13. The voltage reading and a count of the number of ϕ_0 through the loop allows the flux of the external magnetic field to be measured. This is how a SQUID can, in effect, detect fields that are smaller that a flux quantum, which is the smallest measurement of flux. This high sensitivity of SQUIDS is what makes them useful in many different scientific areas.

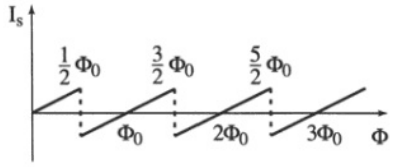

Figure 1.12: Screening current in a SQUID oscillates as a function of applied magnetic flux [5].

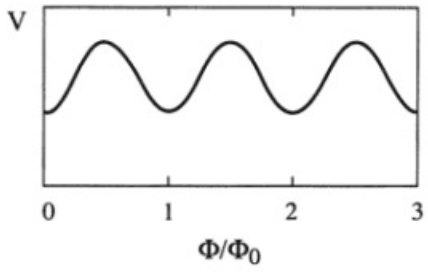

Figure 1.13: Dependence of the SQUID voltage on applied magnetic flux [5].

1.3 SQUID as a Qubit in a Quantum Computer

1.3.1 Brief Introduction to Quantum Computing

Modern day computers work in the classical information regime by manipulating billions of bits of information, which can exist in one of two possible states, 0 or 1. This is the same mechanism that has been around for more than 50 years, since the first computers called Turing machines. Technology continues to advance by adding more and more bits to our current systems, and thus everything is getting smaller and smaller. According to Moore's law, the effectiveness of chip performance doubles every two years. However, the transitiors in our current computers will eventually reach atomic scales, which is the limit of technological advancement.

Unlike our classical computers, quantum computers encode information in quantum bits (qubits) which are a superposition of 0 and 1 states. The power of quantum computing is that this superposition of qubits allows for millions of computations to be performed simutaneously. The qubit state is a complex vector in two dimensional Hilbert space. It is written as a linear combination of the two states, $|0\rangle$ and $|1\rangle$ states, which form an orthogonal basis for the space. The qubit state is given by

$$|\psi\rangle = \alpha|0\rangle + \beta|1\rangle \tag{1.58}$$

where α and β are normalization constraints. At all times other than measurement, the qubit resides in an entangled state of $|0\rangle$ and $|1\rangle$. When measured, it is forced into either the $|0\rangle$ or $|1\rangle$ state, with a probability of measurement of $|\alpha|^2$ and $|\beta^2|$ respectively. The qubit can also be represented in three dimensions by the Bloch sphere, shown in Figure 1.14.

The qubit state vector can now be redefined in terms of the angles within the Bloch sphere as

$$|\psi\rangle = \cos(\phi/2)\,|0\rangle + e^{i\theta}\sin(\phi/2)\,|1\rangle. \tag{1.59}$$

Prior to measurement, the qubit can reside in any orientation within the Bloch sphere. The qubit can hold an infinite amount of information, but this is destroyed at measurement as the system can only be observed in two possible states.

There are two models for quantum computation; adiabatic quantum computing and the gate model. Adiabatic quantum computers, discussed further in the next section, work essentially by solving a minimization problem. Qubit states are used to

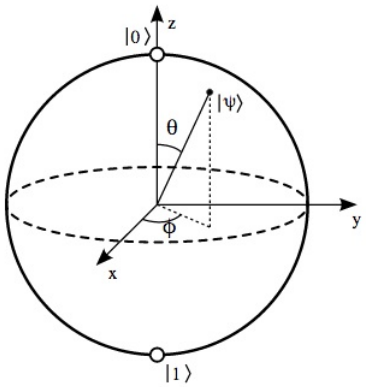

Figure 1.14: A physical representation of a qubit in the Bloch sphere.

represent all possible solutions to a question that is asked, with the correct solution given by the state corresponding to the lowest energy. In the gate model, analogous to classical computers where gates are used to manipulate bits, quantum gates act on qubits and are designed to maximize the probability that the output is the answer required. It is here where we see how quantum computers are useful, as they can simulataneously represent all outcomes of a computation. The end measurement will destroy the superposition and force the state into one outcome. The ability to work on many classical states at the same time is what makes quantum computers important for use in operations that would take infeasible amounts of time on modern day computers. For example, quantum computers will be valuable in factoring large numbers which will aid in the decoding and encoding of secret information.

The first theoretical framework for a quantum computer was proposed in 1982 by Paul Benioff[2]. Benioff constructed the steps of computation in a regular computer on a lattice of spin-1/2 systems using quantum operations. The system naturally does not dissipate much energy due to reversibility of quantum mechanical uniterary operators which form the gates. Prior to this development, Richard Feynman suggested that due to complexity, a computer that runs based on quantum mechanics may be the only way to simulate quantum phenomena[10]. Since then, there has been great progression in the world of quantum computing. David Deutsch designed the first universal quantum computer in 1985, which is an abstract system that models any quantum algorithm[4]. In 1992, Peter Shor developed a factoring algorithm for large numbers, greatly increasing the interest of the public in quantum computers[28]. In classical computers, the time taken to factor large numbers is proportional the exponential of the length, e^L, whereas in quantum computers, the time is proportional

to L^2, meaning that numbers can be factored much faster quantum mechanically, allowing for any codes encrypted classically to be broken. In the next few years, many groups worked on developing the quantum computer experimentally. Daniel Loss and David P. DiVencenzo came up with one of the first notable experimental designs in 1998[18]. The Loss-DiVincenzo quantum computer uses the spin states of coupled single electron quantum dots as the qubits. Another experimental design that emerged in 1998 is by Bruce Kane, who designed a system using qubits as electron donor's nuclear spin states situated within a silicon substrate[15]. Since then there have been many other experimental developments, with different ideas of what to use as qubits. D-Wave Systems Inc, a company based in Vancouver, aims to create quantum computers which use SQUIDs as their qubits. This type of qubit is called a flux qubit and will be described in the next chapter.

1.3.2 SQUID as a Flux Qubit

As explained previously, when a SQUID is subject to an external magnetic field, a screening current is generated around the loop. The direction of the screening current adjusts to ensure that the total flux enclosed in the loop is always a multiple of one flux quantum. To do this, the current changes direction every half integer multiple of Φ_0. The two current directions, clockwise and counter clockwise, define two different states with different energy levels that can be used as basis states. Figure 1.15 is a representation of these two states based on the direction of the supercurrent through the SQUID.

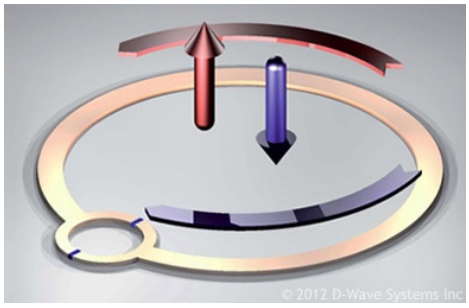

Figure 1.15: Two directions of supercurrent, clockwise, and counterclockwise in a SQUID are used as basis states for a flux qubit.

A simpler version of a DC-SQUID described in the previous section, is a rf-SQUID, which is a loop of superconducting material with only one Josephson junction, as

shown in Figure 1.16. By coupling a coil to the rf-SQUID loop and applying an AC voltage to the coil, one obtains the same flux to voltage conversion observed in the DC-SQUID. Here I will described how a rf-SQUID can become a model two-level system for use as a qubit.

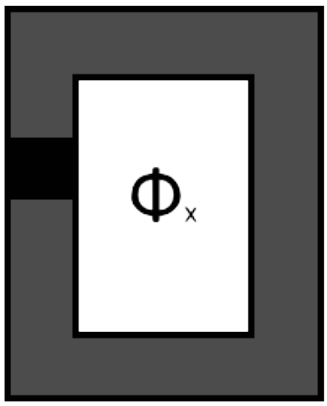

Figure 1.16: The rf-squid is a superconducting loop interupted by a single Josephson junction. an external bias flux Φ_X controls the level separation between the qubits.

The total energy of the rf-SQUID is composed of the Josephson energy, magnetic energy, and electrostatic energy. Thus, the Hamiltonian for the system is given by

$$H = -E_J \cos(\phi) + \frac{1}{2}LI^2 + \frac{1}{2}CV^2\,, \tag{1.60}$$

where L is the inductance of the superconductor, and I is the current through the loop. We can write this in terms of the flux Φ, by noting that due to quantum interference (the Arahanov-Bohm Effect) as in Eq. 1.52, the phase difference across the junction is related to the flux according to

$$\phi = 2\pi\left(\frac{\Phi}{\Phi_0} + \text{integer}\right)\,. \tag{1.61}$$

We can also use the definition of the inductance

$$\Phi = \Phi_X + LI\,, \tag{1.62}$$

and

$$V = \frac{Q}{C} = \frac{2en}{C} \tag{1.63}$$

where C is the capacitance of the junction. From the $\hat{n}$ relation:

$$\hat{n} = i\frac{\partial}{\partial\phi} = \frac{i}{\left(\frac{2\pi}{\Phi_0}\right)}\frac{\partial}{\partial\Phi} = \frac{i\hbar}{2\pi e}\frac{\partial}{\partial\Phi} = \frac{i\hbar}{2e}\frac{\partial}{\partial\Phi}\,, \tag{1.64}$$

we have

$$Q = (2e)\hat{n} = i\hbar\frac{\partial}{\partial\Phi}\,. \tag{1.65}$$

Plugging in all of this to Eq. 1.60 gives

$$H = -E_J\cos\left(\frac{2\pi\Phi}{\Phi_0}\right) + \frac{(\Phi-\Phi_X)^2}{2L} - \frac{\hbar^2}{2C}\frac{d^2}{d\Phi^2}\,. \tag{1.66}$$

Now defining $x = 2\pi\frac{\Phi}{\Phi_0}$ and $x_X = 2\pi\frac{\Phi_X}{\Phi_0}$ such that when $\Phi_X = \Phi_0/2$ we get $x_X = \pi$, we can write

$$\frac{H}{E_0} = -\beta_L\cos x + \frac{1}{2}(x-x_X)^2 - \frac{\hbar^2}{2m^*}\frac{d^2}{dx^2}\,, \tag{1.67}$$

which is in the form of

$$\frac{H}{E_0} = U(x) - \frac{\hbar^2}{2m^*}\frac{d^2}{dx^2}\,. \tag{1.68}$$

Here, $E_0 = \frac{1}{L}\left(\frac{\Phi_0}{2\pi}\right)^2$ with dimensions of energy, and $m^* = \frac{c}{L}\left(\frac{\Phi_0}{2\pi}\right)^2$ with dimensions of $\hbar^2$. When $\Phi_x = \frac{\Phi_0}{2}$, the potential energy is given by

$$U(x) = \beta_L\cos(x-\pi) + \frac{1}{2}(x-\pi)^2\,, \tag{1.69}$$

so for $x' = (x-\pi) \ll 1$, this expands to

$$\begin{aligned} U(x') &= \beta_L\left[1 - \frac{x'^2}{2} + \frac{x'^4}{4!} + O(x'^6)\right] + \frac{1}{2}x'^2 \\ &= \beta_L - \frac{1}{2}(\beta_L - 1)x'^2 + \frac{1}{4!}x'^4 + O(x'^6)\,. \end{aligned} \tag{1.70}$$

Thus for $\beta_L \geq 1$, the rf-SQUID forms a double well potential near $x = \pi$ ($\Phi = \Phi_0/2$). The energy eigenstates of the system will be the following:

$$|0\rangle = \frac{1}{\sqrt{2}}(|R\rangle + |L\rangle) \tag{1.71}$$

and

$$|1\rangle = \frac{1}{\sqrt{2}}(|R\rangle - |L\rangle)\,, \tag{1.72}$$

as represented in Figure 1.17.

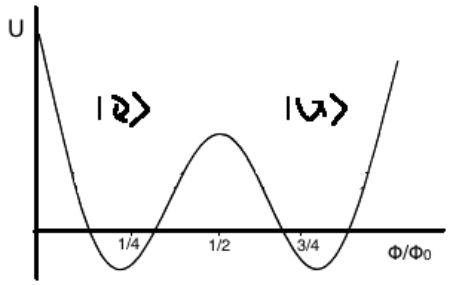

Figure 1.17: Potential energy of a SQUID. When the SQUID is biased near ($\Phi = \Phi_0/2$), the energy forms a double potential well. The two states corresponding to counter clockwise and clockwise directions of the SQUID current can be used as basis states for a qubit.

Here, the state $|R\rangle$ corresponds to a clockwise supercurrent that produces $\frac{-\Phi_0}{4}$ against the external flux to ensure that the total flux enclosed in the loop is a mulitple of Φ_0. The state $|L\rangle$ represents a counterclockwise current, which produces $\frac{\Phi_0}{4}$ to add to the external flux.

By applying a pulse to the SQUID with a frequency that corresponds to an energy equal to the difference between these two energy levels, the SQUID can be put into a superposition of the two states and can act as a qubit. Additional pulses of varying frequencies can be used as quantum gates to adjust the probability of measurement in each of the two states.

1.4 The D-Wave Quantum Computer

D-Wave Systems Inc. is a quantum computing company based in Burnaby, BC that was founded in 1999. D-Wave may be the first company to construct and market a functional quantum computer. Inside the D-Wave quantum computer, the processor consists of many rf-SQUID flux qubits and couplers. The couplers connect two SQUIDs together via induction. A programmable magnetic memory is constructed by circuitry around the qubits and couplers, allowing users to program specific problems into the device.

The D-Wave quantum computer works based on the adiabatic model for quantum computation. The system is intialized into the ground state of a simple Hamiltonian. From there, the Hamiltonian is adiabatically evolved into the ground state of a more complex Hamiltonian, which gives the solution to the problem of interest. In quantum mechanics, the adiabatic theorem states that when evolved over time, a time-dependent Hamiltonian will remain in the lowest energy level as long as the evolution is slow enough. To examine the condition needed for adiabatic evolution to occur, we can start by looking at the Schrödinger equation:

$$i\frac{d}{dt}|\psi(t)\rangle = H(t)|\psi(t)\rangle\,. \tag{1.73}$$

When the Hamiltonians commute such that $[H(t_0), H(t)] = 0$, the time evolution operator is given by

$$U(t, t_0) = e^{-i\int_{t_0}^{t} H(t)dt}\,. \tag{1.74}$$

Over a total evolution time T, we can parameterize the Hamiltonian with a dimensionless parameter $s\epsilon[0, 1]$. The Schrödinger equation then becomes

$$i\frac{ds}{dt}\frac{d}{ds}|\psi(s)\rangle = H(s)|\psi(s)\rangle \tag{1.75}$$

or

$$\frac{d}{ds}|\psi(s)\rangle = -i\frac{dt}{ds}H(s)|\psi(s)\rangle\,. \tag{1.76}$$

We can now define a factor $\tau(s) = \frac{dt}{ds}$, which is called the "delay factor", and is used to describe the speed of evolution of the Hamiltonian. This gives

$$\frac{d}{ds}|\psi(s)\rangle = -i\tau(s)H(s)|\psi(s)\rangle\,. \tag{1.77}$$

It can be shown that in order for the system to be adiabatic, the delay factor must satisfy

$$\tau(s) \gg \frac{||\frac{d}{ds}H(s)||^2}{g(s)^2}\,, \tag{1.78}$$

where $g(s)$ is the energy gap between the ground state and the first excited state [1, 7]. When this condition is met, the system will remain in the ground state at all times. When this condition is not met, diabatic transitions may occur in which the

system jumps into the next excited state.

The computers at D-Wave use this adiabatic process to solve quadratic unconstrained binary optimization (QUBO) problems. These problems happen to be quite important, because they can be show to be members of the important class of nondeterministic polynomial-time hard (NP-hard) problems. Problems in this class are "hard" because the best known algorithms require a time that grows exponentially with the size of the input [31, 11]. Optimization problems are encoded into a Hamiltonian of the form

$$H_{final} = \sum_i h_i \sigma_{iz} + \sum_{i.j} J_{i,j} \sigma_{iz} \sigma_{jz} \,, \tag{1.79}$$

where σ_{iz} is a pauli matrix acting on the ith flux qubit. Its eigenstates are $\sigma_{iz}|L\rangle = +|L\rangle$ and $\sigma_{iz}|R\rangle = -|R\rangle$. Here, h_i, the local bias on qubit i, and $J_{i,j}$, the coupling strength between qubits i and j, are chosen to specify the problem. The system starts in a state described by the initial Hamiltonian

$$H_{initial} = \sum_i h_i \sigma_{iz} + \sum_{i.j} J_{i,j} \sigma_{iz} \sigma_{jz} - \sum_i \delta_i \sigma_{ix} \,, \tag{1.80}$$

where δ_i is a parameter that is adjusted to allow the system to be easily put into the ground state. At $t = 0$, δ_i is set to a value much greater than all h_i's and J_{ij}'s, so that the system can be easily prepared in the ground state: The ground state will be

$$|\Psi(t=0)\rangle = \bigotimes_{i=1}^{N} \frac{1}{\sqrt{2}} \left(|L\rangle + |R\rangle\right) \,. \tag{1.81}$$

From there, the system is evolved adiabatically from $H_{initial} \to H_{final}$ so that $\sum_i \delta_i \sigma_{ix} \to 0$, and the final state will be the ground state of the system with H_{final}. The readout of this state provides the solution to the complex problem.

NP-Hard problems have the property that they can be mapped with polynomial overhead into the most famous class of problems in computer science: The NP-complete problems. An example of NP-complete problem is the travelling salesman problem. With a list of cities at different distances from eachother, this involves finding the shortest possible route in which one can visit each city exactly once and return to the starting point. This may be easy to solve for five or ten cities, but the running time for any classical optimization algorithm increases exponentially with the number of cities. Problems of this type can take unrealistic amounts of time to solve on

everyday computers. The quantum mechanics of D-Wave's device allows the system to reside in all possible solutions at once, and to readout the best solution simply by adjusting parameters until the system falls into the ground state. In this way, adiabatic quantum computing shows great potential for technological advancement. By modelling the problems with the general Hamiltonian in Eq. 1.79, D-Wave's quantum computers can be used to solve problems such as finding correlations in data, labelling and detecting objects in images, and extracting meaning from news stories [22].

Chapter 2

Localized Spins as the Origin of Intrinsic Flux Noise in SQUIDs

2.1 Types of Spin Impurities

The sources of intrinsic noise in SQUIDs are still unknown. However, there are a few possible sources that are thought to affect the results flux measured by the device. Spins near the superconductor produce small magnetic fluctuations. There are two general types of spins that can cause this; electron spins and nuclear spins.

Localized electron spins appear in two distinct ways: dangling bonds [3] and interface states [25]. Dangling-bonds are atomic-like electron states usually associated to vacancy defects in the crystal lattice. In the presence of a vacancy, not all valence electrons of the atom will be singlet-paired to form a covalent bond with other atoms; these electrons are unpaired and possess a magnetic moment. Figure 2.1 illustrates a dangling-bond at the silicon/silicon oxide interface. These are the best understood kind of dangling-bonds; much less understood are dangling-bonds at the niobium/niobium oxide interface. In the next chapter, we will show that these are much more likely to play a role because they are located much closer to the SQUID wire.

Another kind of electron spins that can cause noise is localized states at the metal-insulator interface. In perfect (smooth interfaces), electrons propagate as bloch waves through the metal and are damped in the insulator. Surface roughness causes random fluctuations in the electronic potential at the interface leading to metal-induced gap states (MIGS), which are electron states localized over many atomic lattice sites.

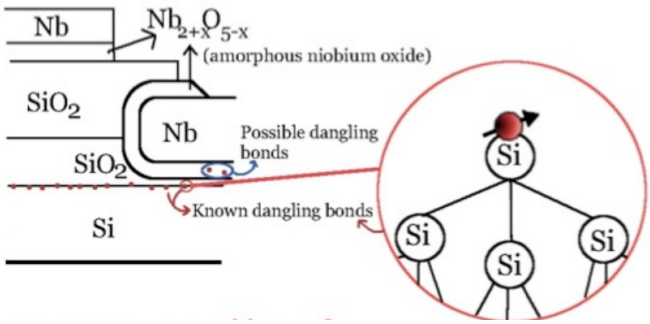

Figure 2.1: A cross-section of the SQUID's Josephson-Junction, showing possible dangling-bonds.

When these MIGS are filled with an odd number of electrons, they possess a magnetic moment and are a source of flux noise in the SQUID [25]. MIGS are expected to appear in the amorphous niobium-oxide layer covering the superconducting metal.

Finally, nuclear spins are always present, even in perfect lattices. While their magnetic moment is approximately 1000x smaller, their density tends to be much higher, so they may play an important role in flux noise.

2.2 Mechanisms of Spin Dynamics

If the spin species discussed in the above section were isolated, they would not fluctuate in time and thus would only produce a static flux offset (or zero-frequency noise). Such a static shift is easy to calibrate-off in the SQUID, and would not cause any problems for its operation. In reality, spins can interact with each other and with the lattice.

Any mechanism that produces spin dynamics will contribute to flux noise. There are two main models that have been proposed to explain the noise that is currently detected in SQUIDs. The first is the single-spin-flip model, that occurs due to the spin-lattice interaction [3]. The second is the spin-diffusion model that occurs due to the mutual spin-spin interactions [9, 8].

In the single spin flip model, one single spin flip will occur, which then induces more spin flips until the magnetization decays to its lowest energy state[3]. This differs from the spin diffusion model in that the magnetization is no longer conserved. Single spin flips can occur due to the spin-orbit interaction and electron-phonon coupling.

The spin-orbit interaction is an interaction of the spin of a particle with its motion.

There is a central force on valence electrons given by

$$V_c(r) = e\phi(r) \tag{2.1}$$

where r is the radial distance from the center of the nucleus, and $\phi(r)$ is the potential due to the nucleus and the negatively charged electrons in the inner shells[26]. The valence electron then feels an electric field of

$$E = -\left(\frac{1}{e}\right)\nabla V_c(r), \tag{2.2}$$

and a moving charge subject to this electric field will experience a magnetic field given by

$$B_{eff} = -\left(\frac{v}{c}\right) \times E\,. \tag{2.3}$$

The spin-orbit interaction potential energy is represented by the following Hamiltonian;

$$H_{LS} = -\vec{m}\cdot B_{eff} = g\mu_B \vec{S}\cdot\left(\frac{v}{c^2}\times E\right) \tag{2.4}$$

where $\vec{m} = 2\mu_B\vec{S}/\hbar$ is the magnetic moment of the electron, and $\mu_B = e\hbar/2m_e$ is the Bohr magneton. This Hamiltonian can be rewritten to show the interaction explicitly as a coupling between the angular momentum operator, $\vec{L}$ and the spin operator $\vec{S}$. Eq. 2.4 becomes

$$\begin{aligned} H_{LS} &= \left(\frac{e\vec{S}}{m_e}\right)\cdot\left[\frac{\vec{p}}{m_e c^2}\times\left(\frac{x}{r}\right)\frac{1}{-e}\frac{dV_c}{dr}\right] \\ &= \frac{1}{m_e^2 c^2}\frac{1}{r}\frac{dV_c}{dr}(\vec{L}\cdot\vec{S})\,, \end{aligned} \tag{2.5}$$

where $\vec{p}$ is the linear momentum of the particle [27].

Phonon-induced transitions in a system can cause an electron to feel a shift in the local spin-orbit interaction. A phonon is the quantum unit of crystal vibration. Interactions of electrons with the lattice can cause atoms to vibrate and spins to flip. Because of this, the magnetization of a polarized ensemble of spins will relax exponentially over time. These changes in the magnetic field and flux create noise in the superconducting device. The spin-lattice interaction with a perfect lattice leads

to a spin flip rate $\Gamma_{lattice} \propto B^5$, where B is the local magnetic field [3]. Because good superconductivity requires $B \approx 0$, SQUIDs operate in a regime where even the earth's magnetic field needs to be compensated so that B is as close to zero as possible. Hence $\Gamma_{lattice}$ is effectively zero and the usual spin-lattice relaxation plays no role. In [3], it was shown that the fluctuations of an amorphous lattice will lead to a finite spin-flip rate $\Gamma_{amorphous}$ even at $B = 0$. This $\Gamma_{amorphous}$ scales as a power law in temperature (typically $T^{2+\alpha}$, with α ranging from 0 to 2, depending on the type and amount of amorphousness of the material. Because the SQUIDs work at the lowest temperatures ($T \sim 0.1$K) it is likely that the single spin-flip process $\Gamma_{amorphous}$ plays a minor role.

At low T and B, it is more likely that the interaction between spins plays a more important role. In the spin diffusion model, double spin flips take place[9]. In this way, the total magnetization is conserved, but the distribution across the width of the superconductor will change. Because the magnetization is conserved, spin diffusion will not cause any noise if the probing magnetic field is uniform. In the case of a SQUID, the current density, which results in a probing magnetic field, is not uniformly distributed across the width of the SQUID. Thus, a change in the magnetization distribution is a significant source of noise, as it will affect the magnetic flux through the loop.

Spins which are coupled to each other can flip through the Ruderman-Kittel-Kasuya-Yosida (RKKY) interaction. The RKKY interaction is an interaction between localized spins, mediated through conduction electrons in the metal. The scattering of conduction electrons is spin dependent. When a conduction electron scatters off a localized electron, its outgoing state is intrinsically connected to the localized electron spin state. This conduction electron then scatters off a second localized electron in another spin dependent scattering process causing an interaction between the localized electron spin states. This interaction is described in the most general form by the Hamiltonian

$$H = \sum_{i<j} J_{RKKY} \vec{S}_i \cdot \vec{S}_j \,, \tag{2.6}$$

where J_{RKKY} is an RKKY coupling factor and $\vec{S}_i$ and $\vec{S}_j$ represent two distinct electron spins. The RKKY interaction always conserves the total spin of the two impurities, hence it can only cause spin-diffusion (not single spin-flips). The magnetization of the spin-field can be written as a sum of delta functions,

$$\vec{M}(\mathbf{r},\mathbf{t}) = \sum_{\mathbf{i}} \tilde{\mathbf{S}}_{\mathbf{i}} \delta(\mathbf{r} - \mathbf{R}_{\mathbf{i}}) \,, \tag{2.7}$$

where each spin is located at $\mathbf{R_i}$, with dimensionless spin operator $\vec{S}_i$. When the spins are coupled by the RKKY interaction, and in the paramagnetic phase where $\langle \vec{S}_i \rangle = 0$, the spin field will satisfy the diffusion equation

$$\frac{\partial \vec{M}}{\partial t} = D\nabla^2 \vec{M} + \zeta \,. \tag{2.8}$$

Here, D is a diffusion constant, and ζ is a random force which drives the spins into thermal equilibrium with themselves. The theory of flux noise due to diffusion is described in detail in our paper [8].

Calculations of the flux due to spins close to the superconductor are done in the next section. We hope they will give insight into reducing noise in SQUIDs.

Chapter 3

Flux Produced by a Single Spin: FastHenry Method

A program called FastHenry was used to begin investigating the flux noise in a SQUID caused by spin impurities. This involves calculating the flux due to a single spin nearby a SQUID, as well as determining the locations of spins that create the greatest amount of flux. In this chapter I will describe how the program works and discuss our results.

3.1 How FastHenry Works

FastHenry is a software package that is used by researchers in academia and in industry to provide electromagnetic solutions to complex problems. First developed at the Massachussetts Institute of Technology, FastHenry is a three-dimensional capacitance and inductance solver. The package provides software for computing the frequency-dependent self and mutual inductances and resistances of conductive structures made of normal metals and superconductors [19]. FastHenry works by solving Maxwell's equations and extracting the inductances and resistances of the conductors in the geometry. It works under the magnetostatic approximation, which assumes that the electric and magnetic fields are both static.

To use the program, information is encoded in a input file to describe the geometry and frequencies of the set up of conductors. Each conductor is divided into rectangular sections, that can then be divided into smaller filaments. The filaments are assumed to have uniform current across the segments. In this way, high-frequency effects

which cause the current to be non-uniform can still be modelled as an approximation by dividing the conductor into many small filaments. The frequency response is calculated in the frequency domain, and then an FFT or a Laplace transform is used to obtain a behavioural description in the time domain[19]. Following this, a convolution is applied to get the temporal response of the circuit. The results of FastHenry are given in a Maxwell Impedence matrix of the form

$$\mathbf{Z} = \mathbf{R} + i\mathbf{L} \tag{3.1}$$

where $\mathbf{R}$ and $\mathbf{L}$ are matrices, $\mathbf{R}$ representing the resistances of the conductors in the geometry and $\mathbf{L}$ representing the inductance. FastHenry 3.0 provides superconductivity support by solving London's and Maxwell's equations simultaneously to obtain the impedence matrix.

In order to examine the effects of a spin outside of a SQUID, a FastHenry input file was designed to describe the geometry of interest. Because a single spin is a magnetic dipole, and a magnetic dipole is an infinitesimal loop of current, the spin impurity was approximated as a small current loop. As the spin is very small in relation to the SQUID size, the SQUID was modelled as a thin superconducting wire as shown below.

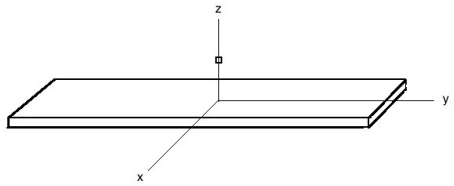

Figure 3.1: A small loop of current outside of a superconducting wire.

With the spin current loop oriented as in Figure 3.1, the magnetic moment points in the $\hat{x}$ direction. By changing the orientation of the current loop, the magnetic moment can be placed in a different direction. When the input file is run through FastHenry, the mutual inductance between the current loop and the wire was extracted and used to calculate the flux induced by the spin on the superconducting wire. This was done using the flux-inductance thereom [Appendix A] which relates the current in the spin loop, I_{spin} to the mutual inductance, M, between the loop and the wire by the equation

$$\Phi = I_{spin} M. \tag{3.2}$$

Based on the fact that the Bohr magneton, $\mu_B = I_{spin}A$ is the magnetic dipole moment of an electron, the flux produced by a single spin becomes

$$\Phi = \frac{\mu_B}{A}M, \tag{3.3}$$

where A is the area of the loop simulating the spin. With this relation, the flux can be calculated directly from the mutual inductance by using the area of the spin loop.

FastHenry provides a reliable method of calculating the flux produced by a tiny loop on a wire of superconducting material. In terms of calculating the flux produced by a single spin on a SQUID, the results are an approximation. Due to size limitations, the approximation becomes less accurate as the distance between the spin loop and the wire approaches the dimensions of the square loop.

3.2 FastHenry: Numerical Results

FastHenry was used as the first method in calculating the flux noise coupled to a SQUID by a single electron spin. As described previously, an input file representing Figure 3.1 was run through the superconducting version of FastHenry, and results were produced which were converted to give the value of the flux. For a single value of z, the distance between the center of the spin loop and the surface of the wire, the flux was calculated as a function of x, the coordinate of the spin loop across the lateral width of the wire. The z-coordinate is perpendicular to the plane of the wire. The center of the wire is at the coordinate $x = 0$. Calculations were done for a superconducting wire of penetration depth $\lambda = 0.07\mu$m, with lateral width $W = 1\mu$m, thickness $b = 0.1\mu$m and wire edges located at $x = \pm 0.5\mu$m. The test spin loop was designed to have a surface area of $A = (0.1\mu\text{m})^2$, with a strip width and a strip height of 0.03μm.

Figure 3.2 shows the calculated flux values for spins located at various distances from a superconducting wire. The variable Φ_x represents the flux in the wire caused by a spin with magnetic moment pointing in the x, or in-plane direction while Φ_z refers to the flux caused by a spin with magnetic moment in the z-direction, perpendicular to the wire. Results for the case where the magnetic moment points in the y-direction are not shown, as all Φ_y values are zero. This can be seen directly from the usual definition of magnetic flux which is given by

$$\Phi = \int_S \vec{B} \cdot \vec{n} da, \tag{3.4}$$

where $\vec{B}$ is the external magnetic field, $\vec{n}$ is a unit vector normal to the wire, and da is the area element. When the spin is in the y direction, $\vec{B}$ is always perpendicular to $\vec{n}$, resulting in zero magnetic flux.

When the magnetic moment is perpendicular along z, the magnitude of the flux is lowest near the center of the wire, and is equal to zero right at the center. The flux direction changes as the spin moves past the center point, so it is expected from symmetry that Φ_z would be zero here. The flux increases towards the edges of the wire where the peaks occur. For the in-plane moment (along x), the flux is also peaked near the edges of the wire. Here, as the flux does not drop to zero at the center of the wire, for spins further away from the wire the flux is quite uniform along the length of the wire, with one central peak. When the spins are closer to the wire, there are two distinguishable peaks. In both cases, the flux increases in magnitude as the spin is moved closer to the wire vertically. The flux drops abruptly to zero when the spin is moved passed the edge and out of the vicinity of the wire.

The results agree with those expected based on the Meissner effect. The internal magnetic field produced by the SQUID loop can only penetrate the superconductor within a penetration depth of the wire's edges, thus the SQUID current flows along the wire edges. The interaction between the spin and the SQUID current will be larger along these edges, thus the flux produced by the spin will peak exactly at the wire edges. The flux calculated for a non-superconducting niobium wire of the same dimensions is shown in Figure 3.2 for comparison. Here, the Φ_x is peaked across the wire for all z-values, as the current is uniform across the wire. It is interesting to note that the Φ_x values differ only slightly in magnitude from the superconducting case. The Φ_z results also show higher values of the flux towards the center of the wire.

Similar calculations were done for the $z = 1\mu$m case by Roger H. Koch, David P. DiVincenzo, and John Clarke in 2007 (they also used FastHenry 3.0) [24]. Our results agree qualitatively with those of Koch et al. reproduced in Figure 3.4. However, the magnitude of our flux values are approximately 30 percent higher than the Koch values, which suggests that the spin loop was closer to the wire than stated in their article.

A problem arises when FastHenry is used to calculate the flux due to spins very close to the superconductor ($z < l_{spin} = 0.1\mu$m, where l_{spin} is the size of the loop

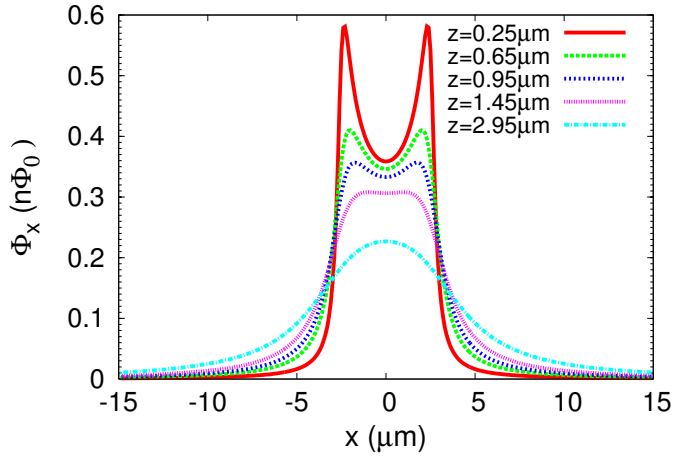

(a) In-plane magnetic moment

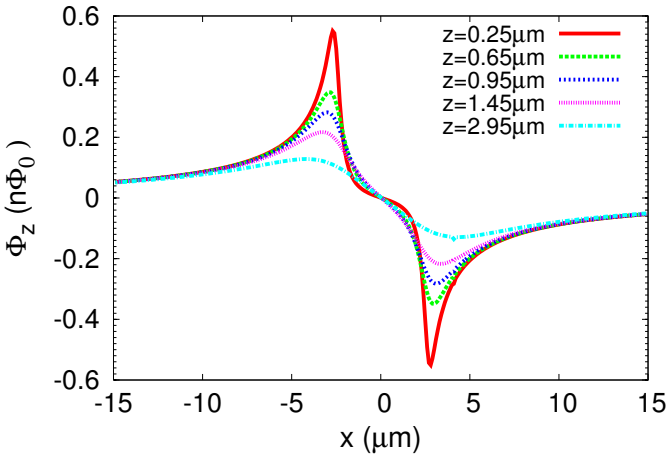

(b) Perpendicular magnetic moment

Figure 3.2: Flux produced by each electron spin impurity as a function of spin location calculated by FastHenry, for a superconducting wire of thickness $b = 0.1\mu$m. The coordinate x runs along the lateral width of the wire, with edges at $x = \pm 2.6\mu$m. The flux is plotted in units of nano flux quanta ($n\Phi_0$).

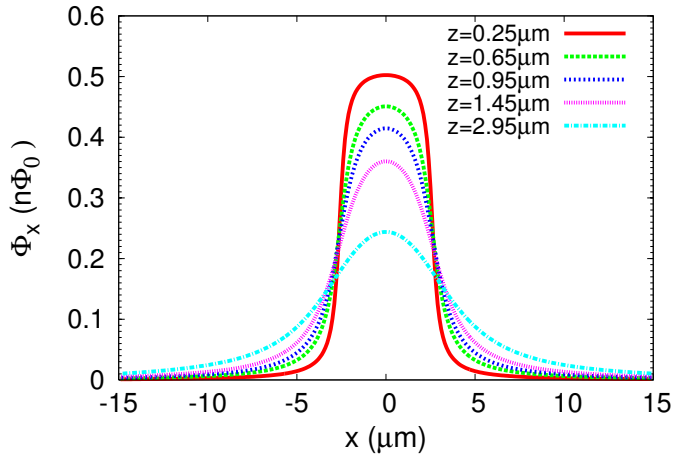

(a) In-plane magnetic moment

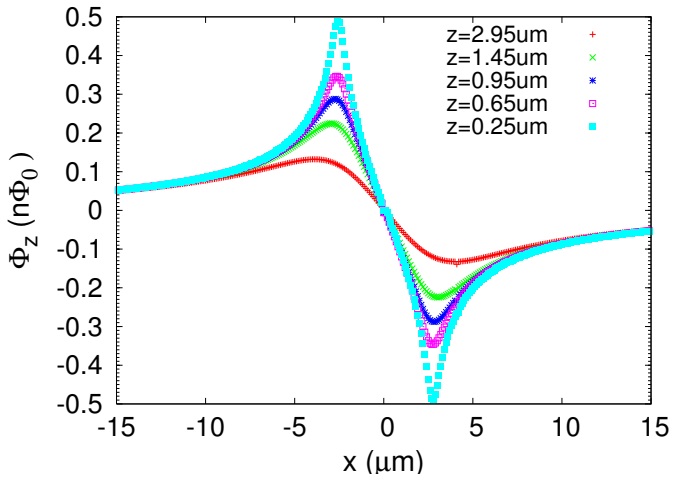

(b) Perpendicular magnetic moment

Figure 3.3: Flux produced by each electron spin impurity as a function of spin location calculated by FastHenry, for a non-superconducting wire of lateral width thickness $b = 0.1\mu$m. The coordinate x runs along the lateral width of the wire, with edges at $x = \pm 2.6\mu$m.

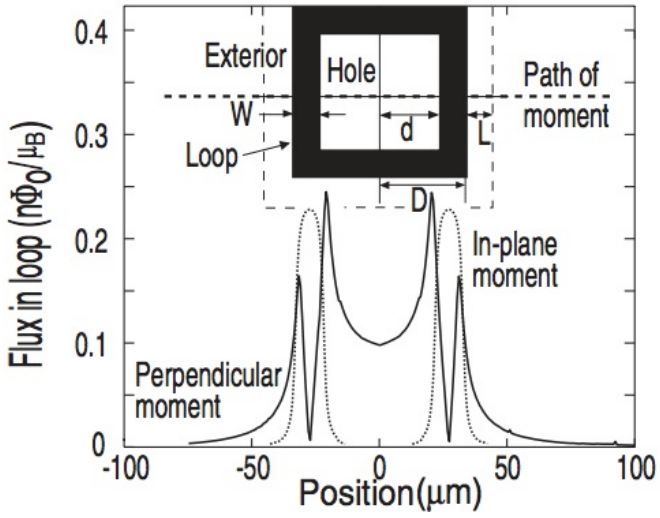

Figure 3.4: Results from Koch, DiVincenzo and Clarke[24] showing the magnitude of the flux per Bohr magneton in the SQUID loop caused by a current loop moving along the path line. Both results for the in-plane and perpendicular moment are given for the SQUID geometry in the inset with dimensions $2D = 52\mu$m and $2d = 41.6\mu$m.

representing the spin). As the spin dipole is being modelled as a loop, it should be as small as possible. Due to length limitations in the software program, the smallest loop that can be designed has an area of $A = (0.1\mu\text{m})^2$. This is a fine for spins further from the wire, but when the distance between the wire is similar to the size of the spin loop, it is no longer a reliable approximation. This is demonstrated in Figure 3.5 which shows the flux produced by spins closer to the wire. Where we would expect the Φ_z peaks to increase in magnitude as the spin is moved closer to the wire, the curves are now identical for all Φ_z values, and even decrease by about 40 percent in comparison to $z = 0.25\mu$m (Compare to Figure 3.2b). The Φ_x peaks also stay fairly constant instead of increasing as z decreases. The breakdown of FastHenry can be seen clearly in the Φ_z plot where there is a gap in flux curve around the edge of the wire.

FastHenry fully accounts for the Meissner effect by solving the London equations, and thus can be used to calculate the flux for a spin near a superconducting wire. The software package gives a very good approximation when the spin is sufficiently far from the wire. The distance between the wire and the current loop must be greater than the dimensions of the square loop used to simulate the spin. For spins closer to the superconducting wire, another method must be used to determine the flux.

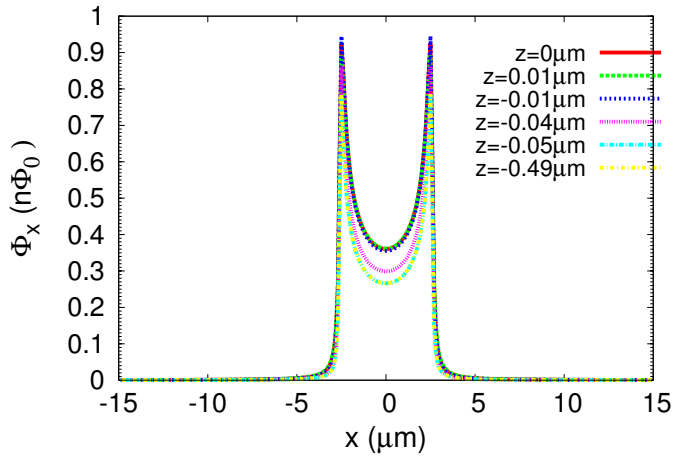

(a) In-plane magnetic moment

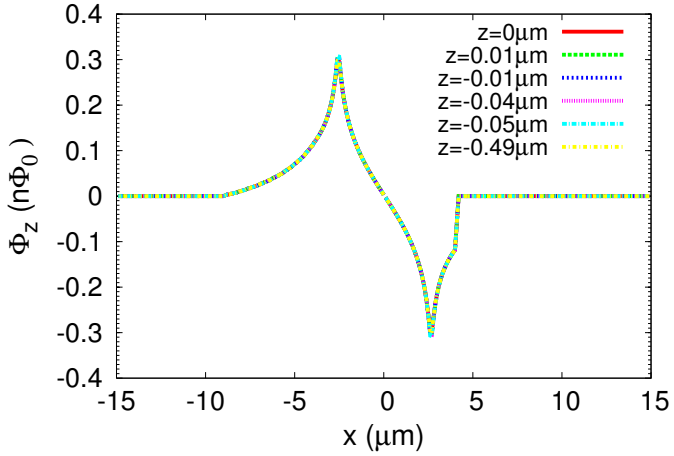

(b) Perpendicular magnetic moment

Figure 3.5: Flux produced by each electron spin impurity as a function of spin location calculated by FastHenry for spins close to the wire. The coordinate x runs along the lateral width of the wire, with edges at $x = \pm 2.6\mu$m.

Chapter 4

Flux Produced by a Single Spin: The Numerical Dipole Method

In the previous chapter, I showed using FastHenry that spins closer to the wire cause a greater flux than spins that are further away from the wire. Because of size limitations in FastHenry, it is necessary to investigate another way of calculating flux noise. Here I present a new method of calculating the flux due to a single spin outside of a SQUID that allows for spin locations at and within the surface of the superconducting wire.

4.1 Theoretical Derivation of the Dipole Method

The Dipole Method is a numerical method of calculating the flux produced by the spin current that is measured by the SQUID current. The interaction energy between the spin and the SQUID is given by

$$H_{spin} = -\vec{m}_i \cdot \vec{B}(\vec{R}_i) \tag{4.1}$$

where $\vec{m}_i = -g\mu_B\vec{S}_i$ is the magnetic moment of the spin, with $\mu_B = |e|\hbar/(2m_e)$ the Bohr magneton, and $g \approx 2$ for electron spins. The magnetic field produced by the SQUID current at the spin's location, $\vec{R}_i$, is

$$\vec{B}(\vec{R}_i) = \frac{\mu_0}{4\pi}\int d^3r \vec{J}_{SQUID}(\vec{r}) \times \frac{(\vec{R}_i - \vec{r})}{|\vec{R}_i - \vec{r}|^3}\ , \tag{4.2}$$

from Jackson's Classical Electrodynamics Eq. 5.14 [13]. The flux is simply given by

$$\Phi_i = \frac{H_{spin}}{I_{SQUID}}\,, \tag{4.3}$$

as proven in the Flux-Inductance Theorem (See Appendix A). This gives

$$\Phi_i = \left[\frac{g\mu_B\mu_0}{4\pi}\int d^3r \frac{\vec{J}_{SQUID}(\vec{r})}{I_{SQUID}} \times \frac{(\vec{R}_i - \vec{r})}{|\vec{R}_i - \vec{r}|^3}\right] \cdot \vec{S}_i \tag{4.4}$$

so that the flux can be written in the form

$$\Phi = \vec{F} \cdot \vec{S}\,, \tag{4.5}$$

and hence we obtain the following expression for the flux vector:

$$\vec{F}(\vec{R}_i) = \frac{g\mu_B\mu_0}{4\pi}\int d^3r \frac{\vec{J}_{SQUID}(\vec{r})}{I_{SQUID}} \times \frac{(\vec{R}_i - \vec{r})}{|\vec{R}_i - \vec{r}|^3}\,. \tag{4.6}$$

An alternate derivation of this method is given in Appendix B which derives the flux vector by using the dipole vector potential directly. Note that F points along the magnetic field produced by the SQUID's current. Hence its direction is given by the right hand rule with the thumb pointing along the SQUID's current. The flux produced by many spins each located at $\vec{R}_i$ with $i = 1, ...N$ is given by

$$\Phi = \sum_i \vec{F}_i \cdot \vec{S}_i. \tag{4.7}$$

For the SQUID set up as shown in Figure 4.1 with the coordinate system defined in Figure 4.2, $\vec{F}_i$ is calculated numerically by using the circular symmetry of the SQUID loop. By symmetry, the component of $\vec{F}_i$ tangential to the loop is zero. In cylindrical coordinates this implies $F_{i\theta} = 0$ so that

$$\begin{aligned} F_{ix} &= F_{i\rho}\cos(\theta) \\ F_{iy} &= F_{i\rho}\sin(\theta) \\ F_{iz}\,. & \end{aligned} \tag{4.8}$$

Thus only two components of $\vec{F}_i$ need to be calculated; $F_{i\rho} = \sqrt{F_{ix}^2 + F_{iy}^2}$ and F_{iz}.

There is no simple analytic form of the current density that can be found by solving the London equations for an isolated, current-carrying, thin superconducting

film. When the thickness of the SQUID wire is comparable to the penetration depth λ, and the width of the wire is much greater than λ, we can assume that the current density is uniform across the thickness of the film. An approximate solution was found for this case[23]. The current density near the center of the strip is given by

$$J_s(x) = J_0(0)\left[1 - \left(\frac{2x}{W}\right)^2\right]^{-1/2}, \tag{4.9}$$

where W is the width of the superconducting wire and x is the coordinate which runs along the width. Near the edges of the superconductor, the current density is

$$J_s(x) = J_s(\frac{1}{2}W)\exp -[(\frac{1}{2}W - |x|)b/a\lambda^2], \tag{4.10}$$

where a is a constant near unity, and is assumed to be equal to 1 here[6]. The two solutions meet at the points

$$x = \pm(\frac{1}{2}W - a\lambda^2/2b). \tag{4.11}$$

The dipole method uses a current distribution of this form, as shown in Figure 4.3. Note that the current is accumulated at the edges of the wire.

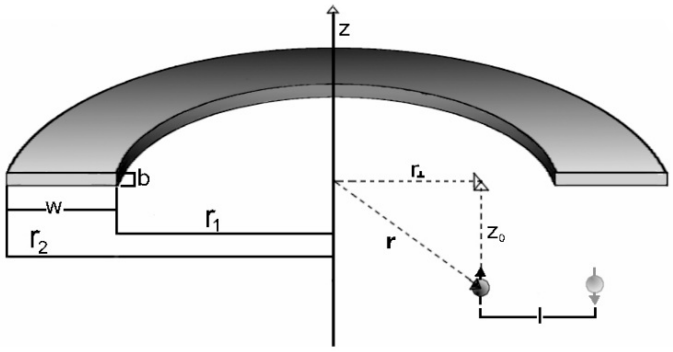

Figure 4.1: The set-up of the SQUID design used in the numerical calculations. The inner and outer radius of the SQUID are labelled by r_1 and r_2 respectively, and here r represents the distance from the centre of the SQUID to the spin impurity.

4.2 Dipole Method: Numerical Results

The numerical dipole method was used to calculate the flux due to a single electron spin impurity near a superconducting wire. The SQUID was set up to have the

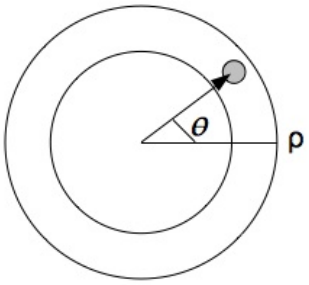

Figure 4.2: The coordinate system used in the F_i calculations. Note that the F_θ component of the flux is always zero due to symmetry (right-hand rule).

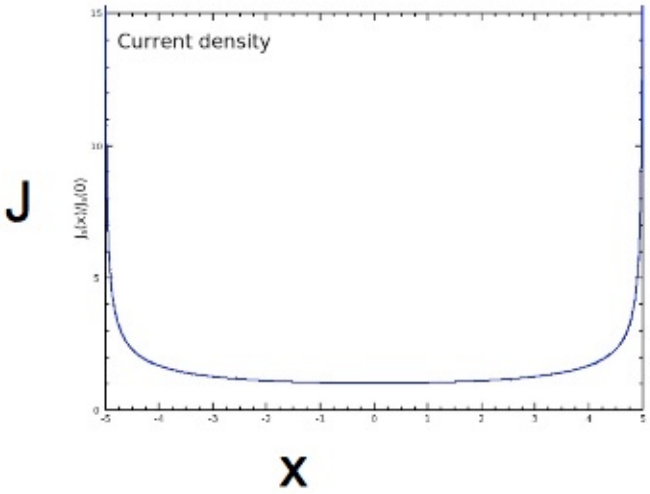

Figure 4.3: The current distribution across of a typical SQUID. The coordinate x runs along the width of the SQUID plane.

same dimensions as used in the FastHenry calculations. The lateral width was set to $W = 5.2\mu$m, and the thickness $b = 0.1\mu$m. Unlike in FastHenry where the spin is approximated to be a small current loop, the dipole vector potential is used to model the spin, and the approximate current distribution Eqs.4.9 and 4.10 is used for $J_{SQUID}(r)$. It should be noted that this current distribution does take into account the Meissner effect for metallic thin films with $b < \lambda$ (because it forces the fields to be approximately zero at $x = W/2$).

However, the numerical dipole method neglects the screening current produced by the spin; in other words, it assumes the field produced by the spin is a perfect dipole as if there was no superconductor nearby. This approximation breaks down for a high density of spins that are ferromagnetically ordered. To see this, assume an ensemble of spins covering the surface of the wire, all of them with magnetic

moment perpendicular to the wire surface. Each spin can be modeled by a small current loop of area A, producing current $I_{spin} = \mu_B/A$. The sum of all these loops will generate a large loop with edge current equal to I_{spin} on one side of the wire, and $-I_{spin}$ on the other. Since the spin areal density $\sigma = 1/A$, we have $I_{spin} = \mu_B\sigma = 1\ \mu A \frac{\sigma}{10^{13}\mathrm{cm}^{-2}}$. This is of similar magnitude to the screening current in typical SQUIDS, where $I_c \sim 1\ \mu A$. Thus, for realistic spin areal densities of the order of 10^{13} cm^{-2}, an ensemble of ferromagnetically ordered spins *will affect the distribution of current in the SQUID*, by making it asymmetrical. Our numerical dipole method is only valid when the ensemble of spins are not oriented along the same direction. This will be true when the spins are in disordered phases such as paramagnetic and spin glass phases (spins oriented randomly), or in an antiferromagnetic phase. The case of ferromagnetism might lead to SQUID current distributions that are quite different from the expressions Eqs. 4.9 and 4.10.

Figure 4.4 shows a comparison of the results from the calculation done using FastHenry and the Dipole method. In the region where FastHenry is credible, i.e. where z>0.1μm, the results from both methods are in close agreement, within 0.01 percent. This is important to note in evaluating the credibility of the results. The fact that the two different methods agree implies that results from the numerical dipole method are reliable and that this method can be used to examine cases with other geometries and parameters, provided that b is not much larger than λ. Note that our $b = 0.1\mu$m is slightly larger than $\lambda = 0.07\mu$m. Thus Figure 4.4 shows that the the approximate current distribution Eqs. 4.9 and 4.10 (valid for $b < \lambda$) is a good approximation for calculating the flux even when b is slightly larger than λ.

The agreement of the results from both methods means that the numerical dipole method can be used to solve our problem of finding the flux due to spins close to the wire. Because there are no size limitations in the program, results where the spin is close to or within the material of the wire are still credible. The calculated Φ_x and Φ_z values are shown in Figure 4.5. Now the Φ_x values increase as the spin is moved closer to the surface of the wire, $z = 0\mu$m, as we would expect. For spins inside the wire, the flux peaks decrease as z approaches the center of the wire which occurs at $z = -0.05\mu$m. At the center of the wire, $\Phi_x = 0$. This makes sense because according the the right hand rule, the flux will change direction at that that point. The Φ_z peaks still remian fairly constant for all z-values. Again for both directions of the magnetic moment, the flux is peaked near the edge of the wire and decreases towards the center.

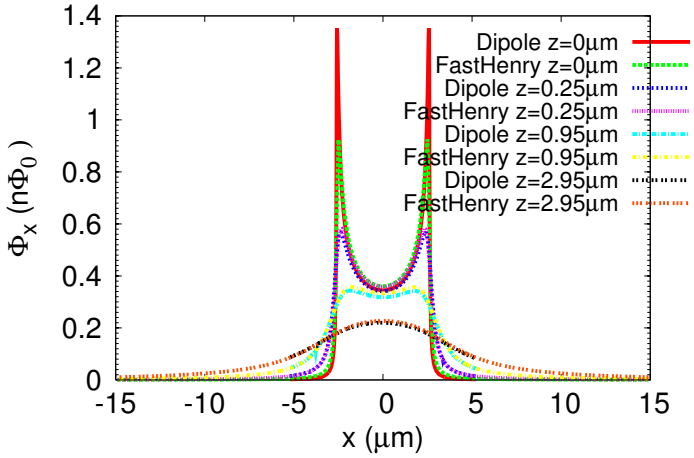

(a) In-plane magnetic moment

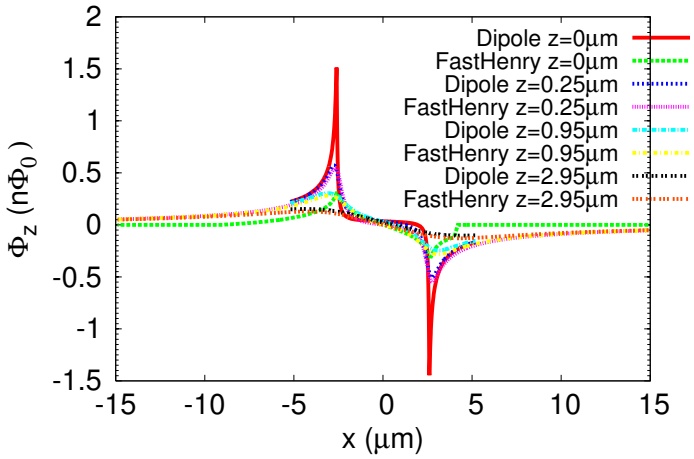

(b) Perpendicular magnetic moment

Figure 4.4: Comparison of the Flux produced by each spin as a function of spin location calculated by FastHenry and the numerical dipole method, for a superconducting wire of thickness $b = 0.1\mu$m. The coordinate x runs along the lateral width of the wire, with edges at $x = \pm 2.6\mu$m.

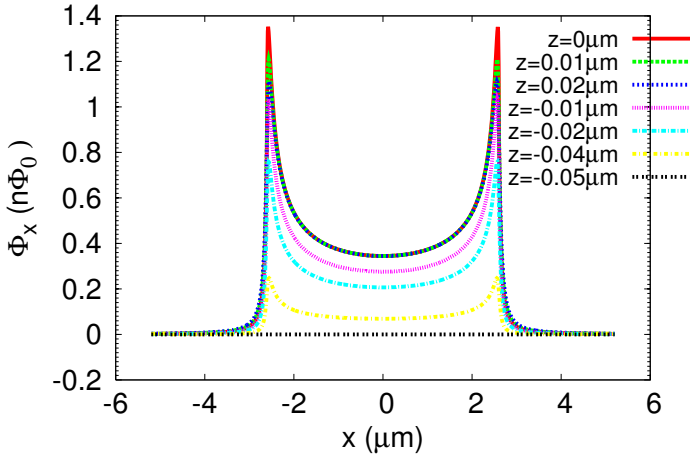

(a) In-plane magnetic moment

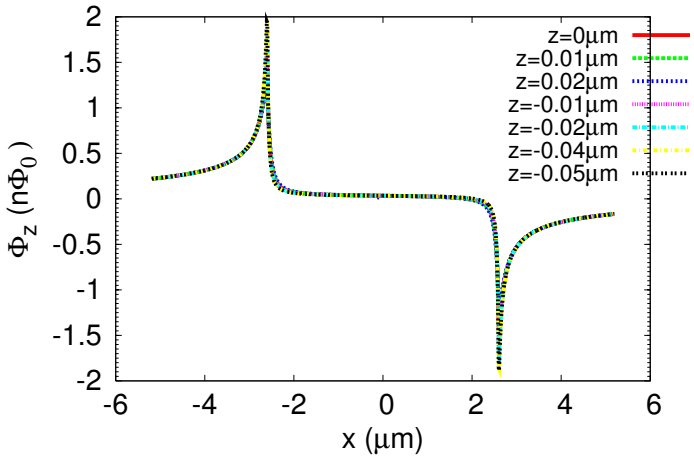

(b) Perpendicular magnetic moment

Figure 4.5: Flux produced by each electron spin impurity as a function of spin location calculated using the numerical dipole method, for a superconducting wire of thickness $b = 0.1\mu$m. The coordinate x runs along the lateral width of the wire, with edges at $x = \pm 2.6\mu$m.

The modulus of the flux vector gives a more useful representation of the flux caused by a single spin. It allows us to compare the magnitude of the flux based on solely the location of the spin, opposed to the spin orientation. Note that for a spin pointing along the $\hat{n}$ direction, $\Phi = \vec{F} \cdot \vec{S} = \vec{F} \cdot \hat{n}/2$, so $\Phi_x = F_x/2$, etc. Because F_y is zero, the modulus of the flux is simply

$$|\vec{F}| = \sqrt{F_x^2 + F_x^2} \ . \tag{4.12}$$

This is shown in Figure 4.6 for a SQUID of the dimensions used in all previous work. When spins are close to the wire, $z \ll W$, or $z \leq 0.1\mu$m in Fig. 4.6, the flux modulus has two distinct peaks near the edge of the wire. The widths of these peaks are of the order of $W/10$. Spins further away from the wire produce a flux that is uniform along the width of the wire, with a slight peak in the center. The maximum flux vector modulus due to a single spin outside the wire is approximately 3.2 nΦ_0.

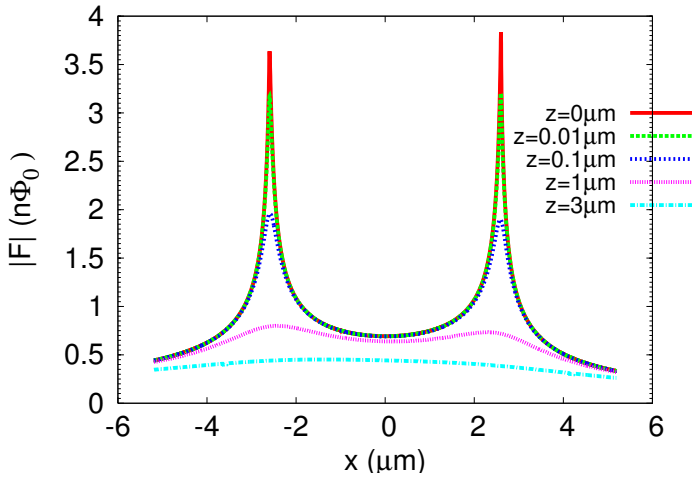

Figure 4.6: Modulus of the flux vector produced by an electron spin impurity as a function of the spin's location, for the superconducting wires of thickness $b = 0.1\mu$m and width $W = 5.2\mu$m.

The quantum computing company DWave Systems Inc. uses SQUIDs of thickness $b = 0.2\mu$m and width $W = 1\mu$m. Figure 4.7 shows the flux profile for the DWave SQUIDs. With a smaller W, the maximum magnitude of $|\vec{F}|$ is now increased to 4.5 nΦ_0. The peaks due to spins close to the wire are less distinct, though the overall shape of the flux modulus differs only slightly from that of the $W = 5.2\mu$m, $b = 0.1\mu$m wire.

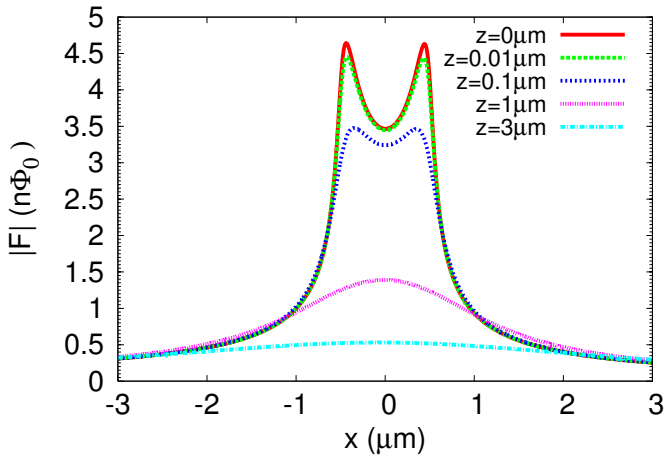

Figure 4.7: Modulus of the flux vector produced by an electron spin impurity as a function of the spin's location, for the superconducting wires in D-Wave's qubits (wire width $W = 1\mu$m and thickness $b = 0.2\mu$m).

Chapter 5

Conclusions

The aim of this thesis was to compute the flux produced by a single spin nearby a SQUID.

First, the software package FastHenry was used to calculate the flux due to a single spin outside of a superconducting wire. The package works by solving the London equations, which accounts for the Meissner effect exactly in the superconductor. This method is an approximation as the spin is represented by a small current loop. FastHenry works effectively for calculating the flux due to spins further from the wire, but because of size limitations in the program, breaks down as the spin is moved closer to the wire.

To further investigate the flux noise due to a single spin close to the SQUID wire, we used a numerical program which uses the exact dipole vector potential to represent the spin. This method does not account for the additional screening current produced by the spin's field, but is a good approximation for an ensemble of randomly oriented spins whose screening current is negligible. Thus, we have a new method to calculate flux which agrees with FastHenry for spins far away from the wire, and does not breakdown for spins close to the superconducting wire. It was found that spins close to the wire cause a flux which is peaked at the wire's edges, with a maximum value of $\sim 4n\Phi_0$ that is 10x larger than previous published calculations based on Fast Henry [24].

Thus we have developed a reliable method for calculating the flux due to a single spin nearby a superconducting wire. We hope that our method will be useful in future efforts to design SQUIDs with lower flux noise.

Bibliography

[1] Dorit Aharonov and Amnon Ta-Shma. Adiabatic quantum state generation. *SIAM J. Comput*, 37:47–82, 2007.

[2] Paul Benioff. Quantum mechanical hamiltonian models of turing machines. *Journal of Statistical Physics*, 29:515–546, 1982.

[3] Rogerio de Sousa. Dangling-bond spin relaxation and magnetic 1/f noise from the amorphous-semiconductor/oxide interface: Theory. *Physical Review B*, 76:245306, 2007.

[4] David Deutsch. Quantum theory, the church-turing principle and the universal quantum computer. *Proceedings of the Royal Society of London A*, 400:97–117, 1985.

[5] É. du Trémolet de Lacheisserie, D.Gignoux, and M.Schlenker. *Magnetism, Materials and Applications*. Springer Science and Business Media, Inc, 2005.

[6] Theodore Van Duzer and Charles W. Turner. *Principles of Superconductive Devices and Circuits Second Edition*. Prentice-Hall, Inc., 1999.

[7] Charles Epstein. Adiabatic quantum computing: An overview. *Quantum Complexity Theory*, 6:845, 2012.

[8] T. Lanting et al. Flux noise in squids: Evidence for temperature dependent spin-diffusion. *arXiv*, 1306.1512, 2013.

[9] Lara Faoro and Lev. B. Ioffe. Microscopic origin of low-frequency flux noise in josephson circuits. *Physical Review Letters*, 100:227005, 2008.

[10] Richard P. Feynman. Simulating physics with computers. *International Journal of Theoretical Physics*, 21:467–488, 1982.

[11] Michael R. Gary and David S. Johnson. *Computers and Intractability: A Guide to the Theory of NP-Completeness*. W. H. Freeman and Company, 1979.

[12] L. N. Cooper J. Bardeen and J. R. Schrieffer. Microscopic theory of superconductivity. *Physical Review*, 106:162–164, 1957.

[13] John David Jackson. *Classical Electrodynamics Third Edition*. John Wiley & Sons, Inc, 1999.

[14] B.D. Josephson. Supercurrents through barriers. *Advances in Physics*, 14:419, 1965.

[15] Bruce E. Kane. A silicon-based nuclear spin quantum computer. *Nature*, 393:133–137, 1998.

[16] Charles Kittel. *Introduction to Solid State Physics, Eighth Edition*. John Wiley & Sons, Inc, 2005.

[17] F. London and H. London. The electromagnetic equations of the superconductor. *Proceedings of the Royal Society of London A*, 149:71–88, 1935.

[18] Daniel Loss and David P. DiVincenzo. Quantum computation with quantum dots. *Physical Review Letters A*, 57:120–126, 1998.

[19] C. Smithhisler M. Kamon, L.M. Siveira and J. White. *FastHenry User's Guide Version 3.0*. Research Laboratory of Electronics, Department of Electrical Engineering and Computer Science, Massachusetts Institute of Technology, 1996.

[20] W. Meissner and R. Ochsenfeld. Ein neuer effekt bei eintritt der supraleitfhigkeit. *Naturwissenschaften*, 21:787–788, 1933.

[21] H.K. Onnes. The resistance of pure mercury at helium temperatures. *Commun. Phys. Lab. Univ. Leiden*, 12:120, 1911.

[22] physicsandcake. Quantum computing and light switches. *Hack the Multiverse D-Wave Blog*, 2011.

[23] E.H. Rhoderick and E.M. Wilson. Current distribution in thin superconducting films. *Letters to Nature*, 194:1167–1168, 1962.

[24] David P. DiVincenzo Roger H. Koch and John Clarke. Model for 1/f flux noise in squids and qubits. *Physical Review Letters*, 98:267003–1–4, 2007.

[25] S.G. Louie S. Choi, D-H. Lee and J. Clarke. Localization of metal-induced gap states at the metal-insulator interface: origin of flux noise in squids and superconducting qubits. *Physical Review Letters*, 103:197001–4, 2009.

[26] J.J. Sakurai. *Modern Quantum Mechanics*. Addison-Wesley Publishing Company, 1994.

[27] Robert Scherrer. *Quantum Mechanics: An Accessible Introduction*. Pearson Education, Inc, 2006.

[28] Peter Shor. Algorithms for quantum computation:discrete logarithms and factoring. *Foundations of Computer Science, 1994 Proceedings, 35th Annual Symposium on*, pages 124–134, 1994.

[29] Michael Tinkham. *Introduction to Superconductivity, Second Edition*. Dover Publications, Inc, 1996.

[30] Frederick C. Wellstood, Cristian Urbina, and John Clarke. Low-frequency noise in dc superconducting quantum interference devices below 1 k. *Journal of Applied Physics*, 50:772–774, 1987.

[31] Wikipedia. Np-hard — Wikipedia, the free encyclopedia, 2013. [Online; accessed 9-July-2013].

Appendix A

Flux-Inductance Theorem

Consider a current loop which encloses an open surface S that has a unit normal $\vec{n}$ as shown in Figure A.1. The magnetic field in the region, $\vec{B}$, is given by $\vec{B} = \nabla \times \vec{A}$.

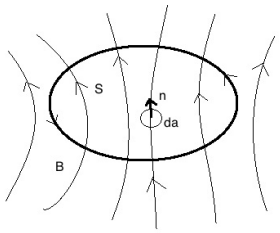

Figure A.1: Magnetic field of an open circuit of current.

The magnetic flux through the circuit of current is defined by

$$\Phi = \int_S \vec{B} \cdot \vec{n} da. \tag{A.1}$$

The Flux-Inductance Theorem relates the Mutual Inductance of current circuits to the flux through the each circuit. The mutual inductance has been defined in Eq. B.10 in relation to the vector potential $\vec{A}(x_i)$ at position x_i in the circuit caused by the current I_j flowing in the jth circuit. If the ith circuit is negligible in cross section compared to the overall scale of both circuits, then the integrand for the integration over the volume of the ith circuit can be reduced to

$$\vec{J}(x) d^3x = J_{||} da dl \tag{A.2}$$

where da is the cross-sectional area differential, and dl is a longitudinal differential in the direction of the current flow. Assuming that the vector potential is constant at

a fixed position along the circuit, this allows the mutual inductance to be written in the form

$$M_{ij} = \frac{1}{I_i I_j} I_i \oint_{c_i} \vec{A}_{ij} dl, \tag{A.3}$$

where the factor I_j comes from the integral of $\vec{J}_{||}$ over the cross section. Using Stokes' Theorem, Eq. A.3 is equivalent to

$$M_{ij} = \frac{1}{I_j} \int_{s_i} (\nabla \times \vec{A}_{ij}) \cdot \vec{n} da \tag{A.4}$$

where $\vec{A}_{ij}$ is the vector potential caused by the jth circuit at the integration point on the ith circuit. Now M_{ij} can be expressed in terms of the magnetic field;

$$M_{ij} = \frac{1}{I_j} \int_{s_i} \vec{B} \cdot \vec{n} da. \tag{A.5}$$

Going back to the definition of magnetic flux, Eq. A.1, the relation between the flux and inductance is given by

$$M_{ij} = \frac{1}{I_j} \Phi_{ij}. \tag{A.6}$$

It can be seen that the magnetic flux through circuit i caused by the circuit j is the product of the mutual inductance of circuits i and j, and the current through the loop j,

$$\Phi_{ij} = I_j M_{ij} \tag{A.7}$$

known as the Flux-Inductance Theorem [13].

Appendix B

Alternate Derivation of the Numerical Dipole Method

In this section we give an alternative derivation of Eq. 4.4, the flux detected by a SQUID due to the presence of a spin nearby its wire. We will show that an interesting subtlety arises with respect to the sign of this expression. Consider a general system of N distinct current-carrying circuits, where the ith circuit has total current I_i. The electromagnetic energy is given by

$$W = \frac{1}{2}\int J \cdot A d^3x\,, \tag{B.1}$$

where J is the current density and A is the magnetic vector potential. Using the expression

$$A(x) = \frac{\mu_0}{4\pi}\int \frac{J(x')}{|x-x'|}d^3x' \tag{B.2}$$

for the vector potential, the energy can be rewritten as

$$W = \frac{\mu_0}{8\pi}\int d^3x \int d^3x' \frac{J(x)\cdot J(x')}{|x-x'|}\,. \tag{B.3}$$

These integrals can now be broken up into sums of separate integrals over each circuit;

$$W = \frac{\mu_0}{8\pi}\sum_{i=1}^{N}\int d^3x_i \sum_{j=1}^{N}\int d^3x'_j \frac{J(x_i)\cdot J(x'_j)}{|x_i - x'_j|}\,. \tag{B.4}$$

The total energy can be expressed as

$$W = \frac{1}{2}\sum_{i=1}^{N} L_i I_i^2 + \sum_{i=1}^{N}\sum_{j>i}^{N} M_{ij} I_i I_j \tag{B.5}$$

where the coefficients L_i and M_{ij} represent the self- and mutual inductances respectively. The sums in Eq. (B.4) contain terms with $i = j$ which define the first sum in Eq.(B.5) and terms with $i \simeq j$ which define the second sum in Eq.(B.5). By comparison of these two forms of W, it can be shown that L_i and M_{ij} are given by

$$L_i = \frac{\mu_0}{4\pi I_i^2}\int_{c_i} d^3x_i \int_{c_i} d^3x_i' \frac{J(x_i)\cdot J(x_i')}{|x_i - x_i'|} \tag{B.6}$$

and

$$M_{ij} = \frac{\mu_0}{4\pi I_i I_j}\int_{c_i} d^3x_i \int_{c_j} d^3x_j' \frac{J(x_i)\cdot J(x_j')}{|x_i - x_j'|}. \tag{B.7}$$

Now, consider the SQUID as a loop with current I_1 and the spin as an infinitesimal loop with current I_2 as show in Figure B.1.

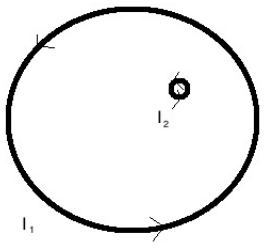

Figure B.1: The large loop carrying current I_1 represents the circuit of the SQUID. The spin circuit is represented by the small loop with current I_1.

For two distinct circuits, the mutual inductance of the two current loops becomes

$$M_{12} = \frac{\mu_0}{4\pi I_1 I_2}\int_{c_1} d^3x_1 \int_{c_2} d^3x_2 \frac{\vec{J}_1(\vec{x}_1)\cdot\vec{J}_2(\vec{x}_2)}{|\vec{x}_1 - \vec{x}_2|}. \tag{B.8}$$

Using the general form of the vector potential,

$$\vec{A}_2(\vec{x}_1) = \frac{\mu_0}{4\pi}\int d^3x_2 \frac{\vec{J}_2(\vec{x}_2)}{|\vec{x}_1 - \vec{x}_2|}, \tag{B.9}$$

the mutual inductance can be defined in terms of J and A and is given by

$$M_{12} = \frac{1}{I_1 I_2} \int_{c_1} d^3x_1 \vec{J}_1(\vec{x}_1) \cdot \vec{A}_2(\vec{x}_1). \tag{B.10}$$

The flux produced by the spin current that is measured by the SQUID current is determined by

$$\Phi = I_2 M_{12}. \tag{B.11}$$

If the spin circuit simulates a true spin, its vector potential must have the exact dipole form:

$$\vec{A}_2(\vec{x}_2) = \frac{\mu_0 \mu_e}{4\pi} \frac{\vec{S} \times (\vec{x} - \vec{R})}{|\vec{x} - \vec{R}|^3}, \tag{B.12}$$

where $\vec{R}$ is the location of the spin, $\mu_e = -g\mu_B$ where $\mu_B = |e|\hbar/2m_e$ is the Bohr magneton, and $\vec{S} = 1/2(\sigma_x, \sigma_y, \sigma_z)$ is the spin operator. Now the flux is given by

$$\begin{aligned} \Phi &= \frac{\mu_0 \mu_e}{4\pi} \int d^3x \frac{\vec{J}_1(\vec{x})}{I_1} \cdot \left[\frac{\vec{S} \times (\vec{x} - \vec{R})}{|\vec{x} - \vec{R}|^3} \right] \\ &= \vec{S} \cdot \left(-\frac{g\mu_0 \mu_B}{4\pi} \int d^3x \frac{(\vec{x} - \vec{R})}{|\vec{x} - \vec{R}|^3} \times \frac{\vec{J}_1(\vec{x})}{I_1} \right), \end{aligned} \tag{B.13}$$

Interestingly, this result differs from Eq. 4.4 by a minus sign. The origin of this minus sign is explained in the end of section 5.16 of [13]. The point is that our Eq. B.1 describing magnetic energy also includes a contribution from "producing the spin circuit", i.e. switch the spin current from zero to its value I_2. This contribution turns out to be equal to the energy required to flip a spin interacting with the SQUID, so that the correct flux is actually -1 times Eq. B.13, identical to our previous Eq. 4.4.